

FINAL REPORT

Project Title: P47 Development of an Advanced Performance Model

for Unbound Granular Pavements 2016/17

ARRB Project No: PRP16021

Author/s: Jeffrey Lee, Didier Bodin and Zia Rice

Client: Queensland Department of Transport and Main Roads

Date: March 2019

AN INITIATIVE BY:

SUMMARY

This report presents the findings of TMR research project P47 'Development of an advanced performance model for unbound granular pavement.' The report covers Year 1 and Year 2 of the research work. The original scope of the project was to undertake laboratory testing, with the data to be used to develop an advanced material model utilising multi-scale modelling techniques (e.g. discrete element technique).

Following a change of personnel, the objectives of the project were rescoped. Instead of developing a new performance model for unbound granular pavements, available laboratory data was used as input into currently-available models to compare the model predictions with observed field performance.

Internationally, there are different approaches used for the design of granular pavements. Some of the methods consider the permanent deformation of the granular layer itself, while in Australia, the current method does not explicitly consider this failure mechanism. The current Australian approach relies on the use of quality aggregate to limit the permanent deformation (shear failure) within the unbound granular layer. Some of these international methods are briefly compared in this report.

As part of this project, two quarry materials were tested in the laboratory. In addition to the basic aggregate testing, repeat load triaxial (RLT) testing was undertaken to characterise the granular materials under cyclic loading. However, this RLT testing did not investigate the change in material behaviour under different vertical pressure (i.e., a fixed vertical pressure of 750 kPa was applied as per Transport and Main Roads Standard Test Q137). This meant that the number of performance models that the data could be input into was limited.

Based on the available test results, it was found that the Tseng and Lytton model (adopted by the US in the MEPDG) was able to fit the permanent strain data measured in the laboratory successfully. It was also found that there was a reasonable correlation between the predicted permanent deformation and the mean rut depth measured at a field trial site.

The report also presents a sensitivity analysis of the South African Mechanistic Design Analysis Procedure (SAMDAP). Different input parameters were used to predict the required granular pavement thickness to limit the plastic deformation within the granular layer. However, it was not possible to conclude whether the SAMDAP system was more or less conservative than the Austroads empirical design chart. Nevertheless, the approach of considering the permanent deformation from within the granular layer is in line with the MEPDG approach taken in the USA.

While an advanced performance model for unbound pavements has not been developed, work was conducted to explore the potential suitability of adopting an alternative and currently- available performance model instead of the current Austroads approach. Recommendations to continue exploring this alternative are provided.

Although the report is believed to be correct at the time of publication, the Australian Road Research Board (ARRB), to the extent lawful, excludes all liability for loss (whether arising under contract, tort, statute or otherwise) arising from the contents of the report or from its use. Where such liability cannot be excluded, it is reduced to the full extent lawful. Without limiting the foregoing, readers should apply their own skill and judgement when using the information contained in the report.

This page is intentionally left blank

TC-710-4-4-8 Page ii March 2019

CONTENTS

1	INTRODUCTION	1
1.1	Problem Statement	1
1.2	Objective and Revised Project Scope	1
1.3	Report Outline	2
2	LITERATURE REVIEW	3
2.1	Resilient Strain Models 2.1.1 K-Theta Model 2.1.2 Uzan Model (1985) 2.1.3 TU Delft Model (Huurman 1997) 2.1.4 Anisotropic Boyce Model (Boyce 1980)	3 3 4
2.2	Plastic Strain Models 2.2.1 Shake-down Theory 2.2.2 Gidel et al. (2001)	
2.3	Selected Permanent Deformation Model – Tseng and Lytton Model	7
2.4	International Pavement Design Methods	9
3	SENSITIVITY ANALYSIS OF THE SAMDAP METHOD AND COMPARISON WITH THE AUSTROADS EMPIRICAL METHOD	13
3.1	Introduction	13
3.2	Design Examples using mePADS	16
3.3	Summary	19
4	LABORATORY TESTING AND MODEL FITTING OF EXPERIMENTAL DATA	20
4.1	Petrographic Assessment	20
4.2	General Material Characterisation Testing	21
4.3	Static Shear Strength Testing	23
4.4	Wheel-tracking Testing	23
4.5	RLT Test Results	24 24 27 30
5	COMPARISON OF RLT DATA WITH FIELD MEASUREMENTS	34

	ENDIX C		
	ENDIX A		
		S	
		Research	
		nry	
6	SUMM	ARY AND FUTURE RESEARCH PLAN	40
5.2	Summa	ıry	39
		Comparison of Computed and Measured Permanent Deformation	
5.1		s ProcedureVertical Strain-Profile	

TABLES

Table 2.1: Table 3.1:	SAMDAP model parameters according to road class	11
Table 3.1.	model	14
Table 4.1:	Petrographic assessment	
Table 4.2:	Material characterisation data	
Table 4.3:	Result of triaxial testing	
Table 4.4:	Results of wheel-tracking testing	
Table 4.5:	Resilient modulus conditions	
Table 4.6:	Specimen preparation and testing conditions	
Table 4.7:	Summary of the relative dry density, moisture content and degree of	
	saturation of prepared RLT samples	28
Table 4.8:	Summary of the relative dry density, moisture content and degree of	
	saturation of RLT samples	31
Table 5.1:	Material properties of Karreman Type 2.1 and quarry samples for Centenary	
	Highway	
Table 5.2:	Summary of material parameters adopted in the numerical analysis	37
FIGURES		
Figure 2.1:	Theoretical behaviour of unbound materials under repeated cyclic load and	
rigare z. r.	different categories of permanent deformation	5
Figure 2.2:	Example Illustrating the curve-fitting process of RLT axial permanent	
9	deformation vs number of loading cycles	g
Figure 3.1:	Typical friction angle and cohesion for each class of SAMDAP granular material	
Figure 3.2:	Structural life of granular and subgrade soil determined using the SAMDAP method over a subgrade CBR 10%	
Figure 3.3:	SAMDAP granular pavement thickness for different subgrade conditions	
Figure 3.4:	SAMDAP granular pavement thickness for different road category over	
· ·	subgrade CBR 5%	16
Figure 3.5:	SAMDAP granular pavement thickness for different drainage conditions corresponding to category a road with subgrade CBR 10%	
Figure 3.6:	Typical input window of mePADS software	
Figure 3.7:	mePADS design chart corresponding to SAMDAP granular pavement types with subgrade CBR 5%	
Figure 3.8:	Comparison of friction angle and cohesion from the Boral Warrians and	
· ·	Karreman quarry against default values from SAMDAP	19
Figure 4.1:	Grading curves	
Figure 4.2:	Dry density and moisture content conditions (Type 2.1 base material from	
J	Boral Warrians quarry)	25
Figure 4.3:	Porosity and water volume conditions (Type 2.1 base material from Boral	
	Warrians quarry)	26
Figure 4.4:	Dry density and moisture content conditions (Type 2.1 base material from	
	Karreman quarry)	26
Figure 4.5:	Porosity and water volume conditions (Type 2.1 base material from the	
	Karreman quarry)	27
Figure 4.6:	RLT axial permanent deformation vs number of loading cycles (Boral	
	Warrians quarry material DD = 98% MDD _{std.})	28
Figure 4.7:	RLT axial permanent deformation vs number of loading cycles (Boral	
	Warrians quarry material DD = 100% MDD _{std.})	29
Figure 4.8:	RLT axial permanent deformation vs number of loading cycles (Boral	
	Warrians quarry material DD = 102% MDD _{std.})	29

TC-710-4-4-8

March 2019

Figure 4.9:	RLT axial permanent deformation vs number of loading cycles (Boral Warrians quarry material DD = 104% MDD _{std.})	30
Figure 4.10:	RLT axial permanent deformation vs the number of loading cycles (Karreman quarry material DD = 98% MDD _{std})	32
Figure 4.11:	RLT axial permanent deformation vs the number of loading cycles (Karreman quarry material DD = 100% MDD _{std.})	32
Figure 4.12:	RLT axial permanent deformation vs the number of loading cycles (Karreman quarry material DD = 102% MDD _{std.})	33
Figure 4.13:	RLT axial permanent deformation vs the number of loading cycles (Karreman quarry material DD = 104% MDD _{std.})	33
Figure 5.1:	Trial pavement design cross-section depicting variable lower subbase thickness	36
Figure 5.2:	Vertical resilient strain profiles with depth in granular base layer using CIRCLY and APADS	38
Figure 5.3:	Comparison of predicted permanent deformation of granular base layer and the condition data measured in the first 36 months at the Centenary Highway	
	Project	39

1 INTRODUCTION

A major proportion of the road pavements in Queensland are composed of a sprayed bituminous seal or asphalt surfacing over dense layers of blended aggregate (gravel, sand, silt, and clay) constructed over a naturally-occurring soil foundation. Unbound granular pavements are key to the cost-effective provision of road transport infrastructure throughout Australia. Compared to thick asphalt and concrete pavements typically found in urban centres, these pavements are significantly less expensive to construct but do not provide the same load-bearing capacity and performance reliability. The quality of construction and drainage condition is therefore critical to the long-term performance of unbound granular pavements.

1.1 Problem Statement

Recently, the number of unbound granular pavements reaching a terminal serviceability condition before fulfilling the design life has reportedly increased (Siripun, Jitsangiam & Nikraz 2012). The majority of these pavements have failed as a result of permanent deformation in the wheelpath, commonly referred to as rutting. Forensic investigations of selected pavements revealed the shape distortion exhibited at the surface was confined to the uppermost granular layer and not reflected through the depth of the pavement structure. Pavements that were observed to fail prematurely also exhibited shear-related distresses although significant structural capacity was still available (Siripun, Jitsangiam & Nikraz 2012).

Unlike asphalt, concrete and stabilised materials, there are no specific performance criteria for unbound granular layers in the Austroads *Guide to the Structural Design of Road Pavements* (Austroads 2018). The design and management of these structures is based on empirical relationships originally developed in the 1930s that do not directly consider the principal failure mode of permanent deformation within the unbound granular layers. Historically, these empirical relationships contained sufficient conservatism to ensure adequate performance. However, greater traffic volumes, heavier axle loads and variable material sources may have resulted in an increase in premature pavement failures and, as a result, potentially reduced the reliability of the design approach. As a result of the inherent limitations, "there are doubts in whether the output of the Austroads design analysis is precise enough in the current pavement conditions" (Siripun, Jitsangiam & Nikraz 2012).

1.2 Objective and Revised Project Scope

The original objective of this project was to develop a performance model for unbound granular pavement materials in Queensland to supplement the Austroads pavement design guidelines. The current Austroads design method focusses on the provision of adequate granular cover thickness to prevent the loss of shape of the pavement surface caused by overstressing of the subgrade. The method does not consider the shear failure that may occur within the unbound granular layers themselves.

In the original scope of works, a proposed PhD research study was a central piece of work to achieve the original objective. Following a change of personnel during Year 2 of this project, significant revision to the project scope was required, including the PhD research study no longer being part of the project scope. In addition, the scope of the project had to be changed to reflect the limited amount of laboratory testing data that was collected during Year 1 of the project.

Instead of developing a new advanced performance model, the focus of the project was changed to inputting the available laboratory data into currently-available models and comparing the predicted field performance.

The revised project scope was to:

- investigate the availability of standard laboratory testing methods which would provide required inputs into identified constitutive performance prediction models
- investigate available material models into which material parameters derived from laboratory testing of unbound granular pavement materials could be input
- conduct laboratory characterisation testing of representative Queensland materials
- compare the design of pavements determined using the current Austroads method with an alternative design approach
- conduct finite element numerical model simulations (e.g. APADS) of pavement response to wheel loading
- prepare a final report based on the work conducted, including recommendations and research plan.

1.3 Report Outline

A literature review was conducted as part of this study. Some common resilient (recoverable) and plastic (non-recoverable) strain models are discussed in Section 2. Section 2 also includes a brief review of two international pavement design models which consider shear deformation within the unbound granular layer.

Section 3 reports the results of a sensitivity analysis using both the current Austroads method and the South African Mechanistic Design Analysis Procedure (SAMDAP).

A summary of the laboratory results is presented in Section 4. Laboratory testing was conducted by Queensland Department of Transport and Main Roads (TMR) in Year 1 of this project to characterise two quarry aggregates (Type 2.1 under standard specification MRTS05 (TMR 2018a)) from the Karreman Quarry and the Boral Warrians Quarry.

Section 5 presents the results of Repeat Load Triaxial (RLT) testing which were input into the plastic strain model developed by Tseng and Lytton (1989) to predict the permanent deformation. The deformation was then compared with field condition data available from a recent road reconstruction project in. A summary of the stress analysis data derived using both the linear elastic layer program CIRCLY and finite element analysis program (APADS) is also presented in Section 5.

Finally, Section 6 presented a summary of this project and some recommendations for future research in this area.

2 LITERATURE REVIEW

Resilient (recoverable) deformation and plastic (non-recoverable) deformation are the two types of deformation a granular material will exhibit when subjected to repeated loading (Lekarp, Dawson & Elsevier 1998). Generally, at the end of the design life, the component of resilient deformation is much smaller than the plastic component (Rahman & Erlingsson 2016). The plastic component will typically be manifested as rutting at the pavement surface. The field performance (the accumulation of plastic strain after a certain number of load repetitions) can be predicted using different strain models, and some of them are presented in this section.

2.1 Resilient Strain Models

The resilient response of a material is defined by the resilient modulus, M_R , and Poisson's ratio. Separating the resilient strain into two components, shear strain (ϵ_q) and volumetric strain (ϵ_v), enables the effect of the stress path on the resilient behaviour to be correctly simulated (Araya 2011).

Presented below are four well-known models recognised for modeling the resilient behaviour of unbound granular material. The number of parameters that requires calibration increases from two (K-Theta model) to four (TU Delft and Boyce).

2.1.1 K-Theta Model

The K-Theta model is shown in Equation 1.

$$M_R = k_1 p_a \left(\frac{3p}{p_a}\right)^{k_2}$$

where

 k_1 , k_2 = Material dependent coefficients and exponents

 $p_a = Atmospheric pressure (101 kPa)$

p = Mean stress (kPa)

2.1.2 Uzan Model (1985)

The Uzan model is shown in Equation 3.

$$M_{R} = k_{1} p_{a} \left(\frac{3p}{p_{a}}\right)^{k_{2}} \left(\frac{\sqrt{2(\sigma_{1} - \sigma_{3})^{2} + 4\sigma_{3}^{2}}}{p_{a}}\right)^{k_{3}}$$

where

 k_1 , k_2 , k_3 = Material dependent coefficients and exponents

 p_a = Atmospheric pressure (101 kPa)

p = Mean stress (kPa)

 σ_1 = Major principal stress, normal (kPa)

 σ_3 = Minor principal stress, confining (kPa)

2.1.3 TU Delft Model (Huurman 1997)

The TU Delft model is shown in Equation 5.

$$M_R = k_1 p_a \left(\frac{\sigma_3}{p_a}\right)^{k_2} \left(1 - k_3 \left(\frac{\sigma_3}{\sigma_1^y}\right)^{k_4}\right)$$

where

 k_1 , k_2 , k_3 , k_4 = Material dependent coefficients and exponents

 p_a = Atmospheric pressure (101 kPa)

 σ_1^y = Yield Stress (kPa)

 σ_3 = Minor principal stress, confining (kPa)

2.1.4 Anisotropic Boyce Model (Boyce 1980)

The volumetric and shear strain components of the Boyce Model are shown in Equation 4.

$$\varepsilon_{v} = \frac{\gamma \cdot p^{n}}{p_{a}^{n-1}} \left[\frac{\gamma + 2}{3K_{a}} + \frac{(n-1)}{18G_{a}} (\gamma + 2) \left(\frac{\gamma \cdot q}{\gamma \cdot p} \right)^{2} + \frac{\gamma - 1}{3G_{a}} \left(\frac{\gamma \cdot q}{\gamma \cdot p} \right) \right]$$

$$\varepsilon_{q} = \frac{2p^{*n}}{3p^{n-1}} \left[\frac{\gamma - 1}{3K_{a}} + \frac{(n-1)}{18G_{a}} (\gamma - 1) \left(\frac{q^{*}}{p^{*}} \right)^{2} + \frac{2\gamma + 1}{6G_{a}} \left(\frac{q^{*}}{p^{*}} \right) \right]$$
7

where

 ε_n = Volumetric strain

 ε_a = Shear strain

p = Mean stress (kPa)

 p_a = Atmospheric pressure (101 kPa)

n = Model parameter

 γ = Coefficient of anisotropy

 K_a = Bulk modulus (MPa)

 G_a = Shear modulus (MPa)

q = Deviator stress (kPa)

For the K-Theta, Uzan and TU Delft models, Equation 5 demonstrates how to obtain volumetric strain and shear strain values from the estimated resilient modulus and the Poisson's ratio.

$$\varepsilon_{v} = \frac{\Delta \sigma_{1}}{M_{R}} (1 - 2\nu)$$

$$\varepsilon_q = \frac{2\Delta\sigma_1}{3M_R}(1+\nu)$$

where

 ε_n = Volumetric strain

 ε_a = Shear strain

 $\Delta \sigma_1$ = Change in major principal stress, normal (kPa)

 M_R = Resilient modulus (MPa)

 ν = Poisson's ratio

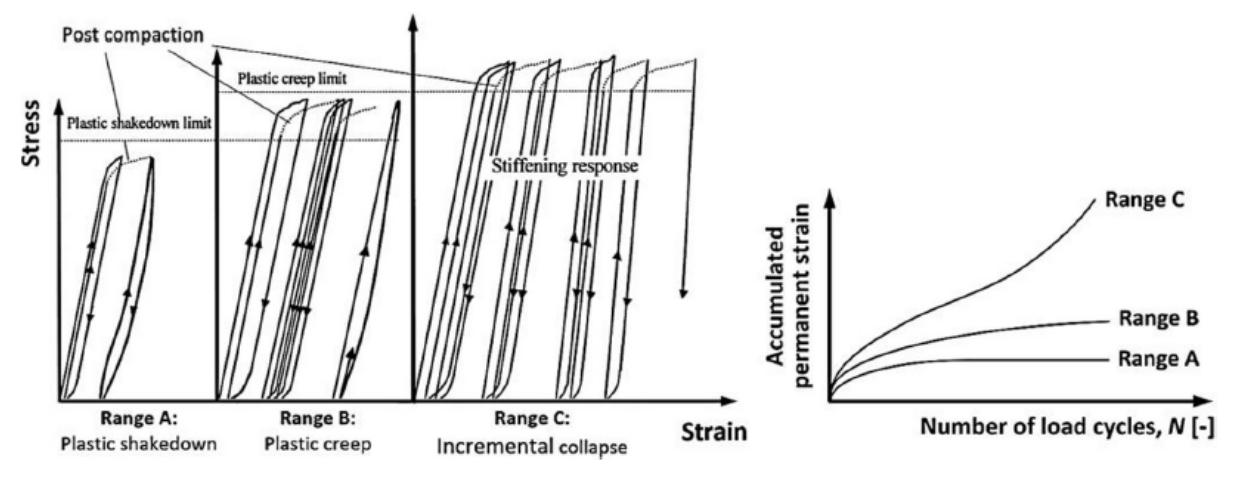
The anisotropic Boyce model is the most reliable for describing resilient behavior. However, it is based on RLT testing where both the axial and the radial strain of the specimen are measured. More commonly, routine RLT resilient modulus testing is based on the axial strain. The k-Theta, Uzan and TU Deft models are therefore better suited to predicting the resilient response of unbound granular materials under various stress conditions.

2.2 Plastic Strain Models

2.2.1 Shake-down Theory

Shake-down theory describes the plastic strain behaviour of pavement materials subjected to repeated loading. It makes a distinction between three types of plastic strain behaviour (Theyse & Kannemeyer 2010). The three ranges of possible behaviour (A, B and C) apply to ascending stress levels respectively. Range A is termed the plastic shake-down range, range B is termed the plastic creep range, and range C is the incremental collapse stage (Erlingsson, Rahman & Salour 2017). A diagram illustrating the different categories of permanent deformation is shown in Figure 2.1.

Figure 2.1: Theoretical behaviour of unbound materials under repeated cyclic load and different categories of permanent deformation



Source: (Erlingsson, Rahman & Salour 2017).

Material falling into range C is considered unsuitable because incremental collapse occurs, causing the permanent strain to increase exponentially. Material falling into range B may be permitted for use under limited load cycles as the long-term plastic strain continues to increase linearly. Material falling within range A is considered the most desirable, as the incremental plastic strain decreases with increasing load cycles until a constant value, or shake-down is reached (Theyse & Kannemeyer 2010). These ranges can be described by the following strain limits (Werkmeister 2004).

$$\begin{split} \left(\varepsilon_{p}^{5000} - \varepsilon_{p}^{3000}\right) &< 0.045 * 10^{-3} & \textit{Range A} \\ 0.045 * 10^{-3} &< \left(\varepsilon_{p}^{5000} - \varepsilon_{p}^{3000}\right) &< 0.4 * 10^{-3} & \textit{Range B} \\ \left(\varepsilon_{p}^{5000} - \varepsilon_{p}^{3000}\right) &> 0.4 * 10^{-3} & \textit{Range C} \end{split}$$

where

 $\varepsilon_{\rho}^{5000}$ = Accumulated strain after 5000 load cycles $\varepsilon_{\rho}^{3000}$ = Accumulated strain after 3000 load cycles

The shake-down theory illustrates the different deformation regimes which can be experienced by an unbound granular material. It provides a framework to predict the range of material behaviour under a given stress state.

The other permanent deformation approaches and models described in the next sections were developed to access the incremental growth of permanent deformation with the repetition of load cycles. These models are based on load cycles, stress levels and stress history (Ahmed & Erlingsson 2013). The material-specific parameters are sensitive to changes in density and moisture content. The model parameters are determined by permanent deformation testing under RLT conditions. They are well suited to fit the increase in plastic strain with loading cycles when the material is tested in Ranges A and B.

2.2.2 Gidel et al. (2001)

$$\varepsilon_p(N) = \beta_1 \varepsilon^0 \left[1 - \left(\frac{N}{100} \right)^{-B} \right] \left(\frac{\sqrt{\left(q_{max}^2 + p_{max}^2 \right)}}{p_a} \right)^n \left(m + \frac{s}{p_{max}} - \frac{q_{max}}{p_{max}} \right)^{-1}$$

where

 ε_p = Permanent strain

 $\beta_1, \varepsilon^0, B, \atop n, m, s$ = Material specific parameters

N = Number of loading cycles

 q_{max} = Maximum deviator stress (kPa)

 p_{max} = Maximum mean stress (kPa)

 p_a = Atmospheric pressure (101 kPa)

2.2.3 Korkiala-Tanttu (K-T), 2005

 $\varepsilon_{p}(N) = \beta_{1}CN^{b} \frac{\frac{q_{max}}{\left(\frac{6ccos\phi + 6p_{max}sin\phi}{3 - sin\phi}\right)}}{1.05 - \left[\frac{q_{max}}{\left(\frac{6ccos\phi + 6p_{max}sin\phi}{3 - sin\phi}\right)}\right]}$

where

 ε_p = Permanent strain

 β_1 , C, b = Material specific parameters

N = Number of loading cycles

 q_{max} = Maximum deviator stress (kPa)

 p_{max} = Maximum mean stress (kPa)

c = Cohesion (kPa)

 ϕ = Angle of internal friction (°)

2.2.4 Tseng and Lytton (1989)

The constitutive relationship is needed to describe the accumulation of permanent deformation in unbound granular materials. Many researchers have developed a mathematical relationship between permanent deformation and the number of load applications. For example, Tseng & Lytton (1989) developed a three-parameter permanent deformation mathematical model to predict the accumulation of permanent deformation with the number of load applications.

The mathematical model was developed based on the results of laboratory permanent axial deformation measurement of a specimen and the number of loading cycles. The relationship is expressed by:

$$\varepsilon_p = \varepsilon_0 \exp\left(-\left(\frac{\rho}{N}\right)^{\beta}\right)$$
 12

where

 ε_p = Axial permanent strain

N = Number of the loading cycle

 ε_0 , ρ , β = Material properties obtained from laboratory testing

The three material parameters, ε_0 , ρ and β , are determined based on the laboratory density, moisture content, resilient modulus and stress states data for different types of base or subgrade materials using multiple regression analysis. A mathematical derivation of this model is included for completeness in Appendix A.

A major advantage of this model is that it has been used to calculate the permanent deformation of unbound granular pavement layers, including laboratory-to-field shift factors, as discussed in Section 2.3.

2.2.5 Rahman and Erlingsson (2016)

$$\varepsilon_p(N) = aN^{\left(\frac{bq_{max}}{p_a}\right)^{\alpha}} \frac{\left(q_{max}/p_a\right)}{\left(\frac{p_{max}}{p_a}\right)^{\alpha}}$$

where

 ε_n = Permanent strain

 a, b, α = Material specific parameters

N = Number of loading cycles

 q_{max} = Maximum deviator stress (kPa)

 p_{max} = Maximum mean stress (kPa)

 p_a = Atmospheric pressure (101 kPa)

Both the Tseng and Lytton and Rahamn and Erlingsson permanent deformation models are based on laboratory RLT testing. Mathematical relationships are fitted to the accumulated permanent deformation with loading cycles data measured under given stress conditions. In addition to RLT testing, static shear testing results are required to calibrate both the Gidel and Korkiala-Tanttu models.

2.3 Selected Permanent Deformation Model – Tseng and Lytton Model

During the project, the materials were tested for permanent deformation under RLT conditions as per Transport and Main Roads Standard Test Q137 (TMR 2017). Testing is performed at a constant vertical pressure of 750 kPa. Testing was conducted at different degrees of saturation to assess the effect of moisture on permanent deformation. The shear strength of the materials was also measured under a limited set of moisture conditions.

By considering the limitations of the available dataset, it was apparent that models requiring the shear strength parameters could not be accurately fitted for the different moisture conditions. The project team therefore decided to adopt the Tseng and Lytton model for inputting the available laboratory data. It is worth noting that this was also the model chosen by the MEPDG developed in the USA (see Section 2.4.1). The laboratory and field deformation data was compared and laboratory-to-field shift factors determined.

The model for pavement design (Equation 14) uses a similar mathematical form, with the vertical resilient strain in the pavement layers calculated. The permanent deformation in a layer is integrated with depth of the layer of thickness h. The total rutting in the pavement structure is the sum of the rutting in each of the susceptible layers (base, subbase, and subgrade).

$$\delta_a = \beta_{GB} \, \frac{\varepsilon_0}{\varepsilon_r} \, exp\left(-\left(\frac{\rho}{N}\right)^{\beta}\right) \times \varepsilon_v \times h$$
 15

where

Deformation of the considered layer δ_a

Thickness of the layer or sub-layer considered h.

N Number of loading cycles

 $\varepsilon_0, \rho, \beta$ Material parameters that are different for each sample

Resilient strain imposed in a laboratory test to obtain the material ε_r

properties, ε_0 , ρ and β (m/m)

Average vertical resilient strain in the layer/sublayer as obtained from the ε_v

pavement response to load model

Laboratory-to-field calibration factor, which is 1.673 for the unbound β_{GR}

granular base, and 1.35 for the subgrade

In the project, the material parameters $(\varepsilon_0, \rho, \beta)$ needed for the above computation were determined by fitting the measured RLT data into the Tseng and Lytton model. An example of the curve fitting process is shown in Figure 2.2. An iterative algorithm was used to arrive at a set of best-fit material parameters (ε_0 , ρ , β) to the measured RLT data. For each compaction effort, moisture content, and density values, a set of material parameters was determined. The fitted material parameters are discussed further in Section 4.5.3 and Section 4.5.4. A full list of the material parameters, and the corresponding coefficient of determination (R²) values, are presented in Appendix B.

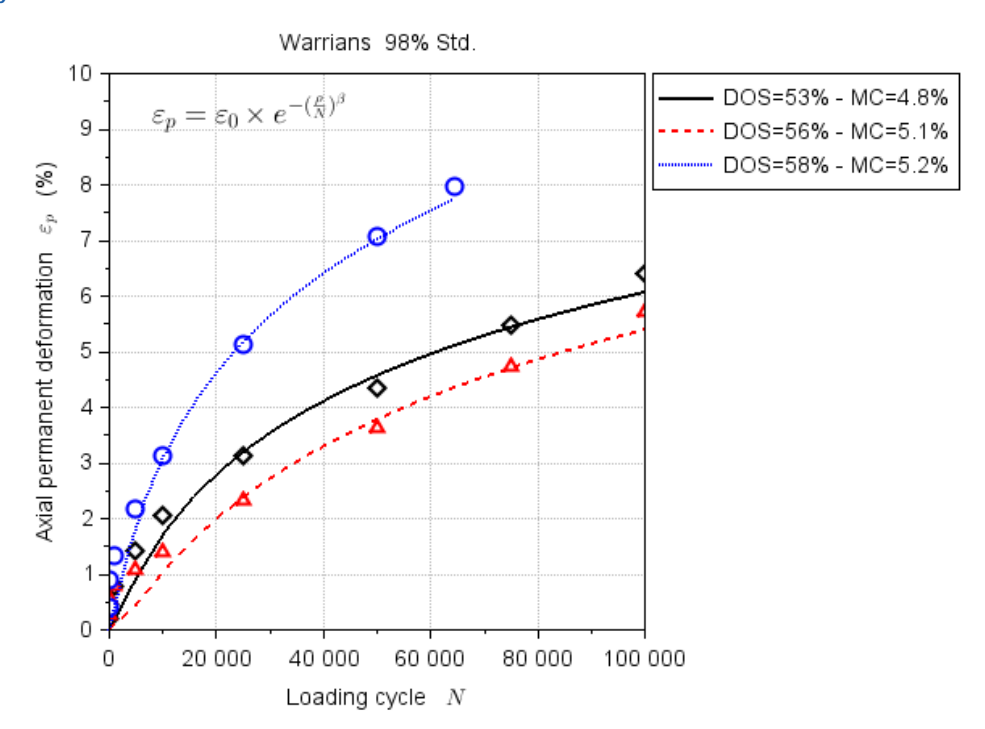


Figure 2.2: Example Illustrating the curve-fitting process of RLT axial permanent deformation vs number of loading cycles

2.4 International Pavement Design Methods

A universal framework for satisfactorily explaining the mechanistic response of unbound granular pavement materials subjected to repeated loading does not currently exist (Lekarp, Dawson & Elsevier 1998). Granular materials play a significant role in the performance of flexible pavements, as the design life is directly related to material quality and response to loading. The four most significant factors controlling the response of granular layers to repeated loading include material quality, relative density, moisture content and the magnitude and number of load applications (Theyse et al. 2007). Consideration of all the factors contributing to a material's response to load must be undertaken if in-pavement performance is to be predicted accurately.

2.4.1 MEPDG

The mechanistic-empirical pavement design guide (MEPDG), also known as NCHRP 1-37, was the result of a multi-year research effort sponsored by the National Cooperative Highway Research Program (NCHRP) in the United States of America. The objective of the MEPDG program was to establish a mechanistic design methodology to replace the American Association of State Highway and Transportation Officials (AASHTO) empirical system that had served as the national standard since 1993. The MEPDG resulted from the combination of numerous investigations related to the long-term performance of pavements including material characterisation, in situ performance, environmental and climate effects, traffic impacts and the development of an advanced finite element method (FEM) numerical response model. The MEPDG was initially released in 2004 for review by state and local road agencies and has been selectively adopted both in-part and wholly throughout the USA.

The prediction of permanent deformation within flexible pavements according to the MEPDG is accomplished by considering the plastic deformation in each layer, relative to a range of traffic loading, climate and moisture content conditions, and summing the total permanent deformation of the composite pavement structure. The permanent deformation of the granular layer in MEPDG

utilises the Tseng and Lytton model. The design of flexible pavements according to the MEPDG includes:

- assembling relevant project constraints (subgrade support, material properties, design traffic, climate, pavement composition, and design and construction features)
- selecting a trial pavement configuration
- establishing terminal serviceability conditions (roughness, rutting, cracking, etc.)
- selecting the desired design reliability
- obtaining monthly traffic, seasonal variability and climate inputs for the entire design period
- computing mechanical responses using either linear-elastic or FEM response models
- calculating accumulated damage and key distress development
- evaluating expected performance relative to design requirements.

The MEPDG pavement response models for unbound granular materials consider vertical compressive stresses and strains within the base and subbase layers in addition to the vertical compressive stresses and strains at the top of the subgrade. This allows for assessment of the permanent deformation potential within each layer separately, with respect to both time and traffic, allowing for design and material optimisation. The permanent deformation model is determined according to Equation 11 discussed in Section 2.3 of this report.

The MEPDG is a complex model and needs to be calibrated for climatic areas and specific procedure. Furthermore, the method utilises a recursive procedure to calculate the determination over the life of the pavement.

Without going through the complex MEPDG software (which the project team does not have access to), the Tseng and Lytton model (also used by MEPDG) was used to compute the permanent deformation of the granular layers and the field condition data. This is discussed in Section 5.

2.4.2 **SAMDAP**

The South African Mechanistic Design Analysis Procedure (SAMDAP) is the culmination of several research efforts conducted in 1977, 1978, 1981 and 1985 and summarised by Theyse et al. (1996). The development and validation of the method was undertaken using both accelerated simulated loading and observations of field performance over a period of approximately 20 years. The method was formally introduced as a standard design method in 1995; it is a component of the South African Mechanistic Design Method documented in TRH4 (Theyse et al. 1996).

The design of unbound granular pavements according to the SAMDAP includes:

- selecting a trial pavement configuration
- characterising pavement materials and traffic loading conditions
- conducting linear elastic analysis
- determining the pavement response parameters
- applying the performance transfer functions
- evaluating expected performance relative to design requirements.

SAMDAP utilises a multi-layer linear elastic model to calculate the critical pavement response parameters (stress/strain). Prediction of the long-term performance of unbound granular pavements includes determining the service life of individual layers (transfer functions) then estimating the ultimate pavement life. Transfer functions are used to evaluate the performance of

individual pavement layers relative to the controlling distress modes. As already discussed, the principle distress mode for unbound granular pavements is permanent deformation as a result of densification and gradual shear under repeated loading (Theyse et al. 1996). The major and minor principal stresses are critical parameters for modeling the mechanistic response of granular layers (Theyse et al. 1996). The allowable loading for unbound granular layers is determined according to Equation 12.

$$N = 10^{2.605122(FS+B)}$$
 16

where

N = Allowable loading (ESA)

FS = Factor of safety against shear failure

B = A constant determined by the road category as presented in Table 2.1

Table 2.1: SAMDAP model parameters according to road class.

Road category	Description	Design reliability	A-factor	B-factor
А	Highway and major urban roads	95%	36.30	3.480098
В	Urban collectors and major rural roads	90%	36.38	3.707667
С	Rural roads	80%	36.47	3.983324
D	Lightly trafficked roads	50%	36.70	4.510819

The factor of safety against shear failure (FS) is determined for each granular material using the Mohr-Coulomb theory for static triaxial loading as shown in Equation 13.

$$FS = \frac{\sigma_3 \phi + C}{(\sigma_1 - \sigma_3)}$$

where

 σ_3 = Minor principle stress, confining (kPa)

 ϕ = Angle of internal friction (°)

C = Cohesion (kPa)

 σ_1 = Major principle stress, normal (kPa)

Similar to the unbound granular material, the principle distress mode for subgrade materials is the permanent deformation resulting from the application of repeated traffic loads (Theyse et al. 1996). The critical mechanical response for the estimation of permanent deformation in the subgrade is the maximum vertical compressive strain at the subgrade surface, similarly to both the Austroads and MEPDG methods. The amount of permanent deformation in the subgrade is determined according to Equation 14.

$$N = 10^{\left(A - 10LOG(\varepsilon_{v})\right)}$$
 18

where

N = Allowable number of load applications (ESA)

A = A constant determined by road category (see Table 2.1)

 ε_{v} = Maximum vertical compressive strain in (μ m/ μ m)

The A-factors presented in Table 2.1 are relative to a terminal serviceability condition of 20 mm of permanent deformation. The ultimate pavement life is the lesser of the allowable loading values determined according to Equations 12 and 14.

3 SENSITIVITY ANALYSIS OF THE SAMDAP METHOD AND COMPARISON WITH THE AUSTROADS EMPIRICAL METHOD

3.1 Introduction

The SAMDAP model determines the structural capacity of each layer in the pavement. The overall structural capacity of the pavement is governed by the critical layer that has the highest damage, resulting in the shortest pavement life. In a granular pavement, both the granular layer and the subgrade contribute to the permanent surface deformation. The SAMDAP assumes that the permanent deformation within the granular layer was caused by shear deformation. The state of shear stress is determined in the middle of each granular layer. The granular layer is characterised by cohesion and friction angle, determined using the Mohr-Coulomb model. Each class of granular material has a default value for cohesion and friction angle as shown in Figure 3.1. The subgrade layer also develops permanent deformation. The rutting of the subgrade is a function of the vertical compressive strain at the top of the layer.

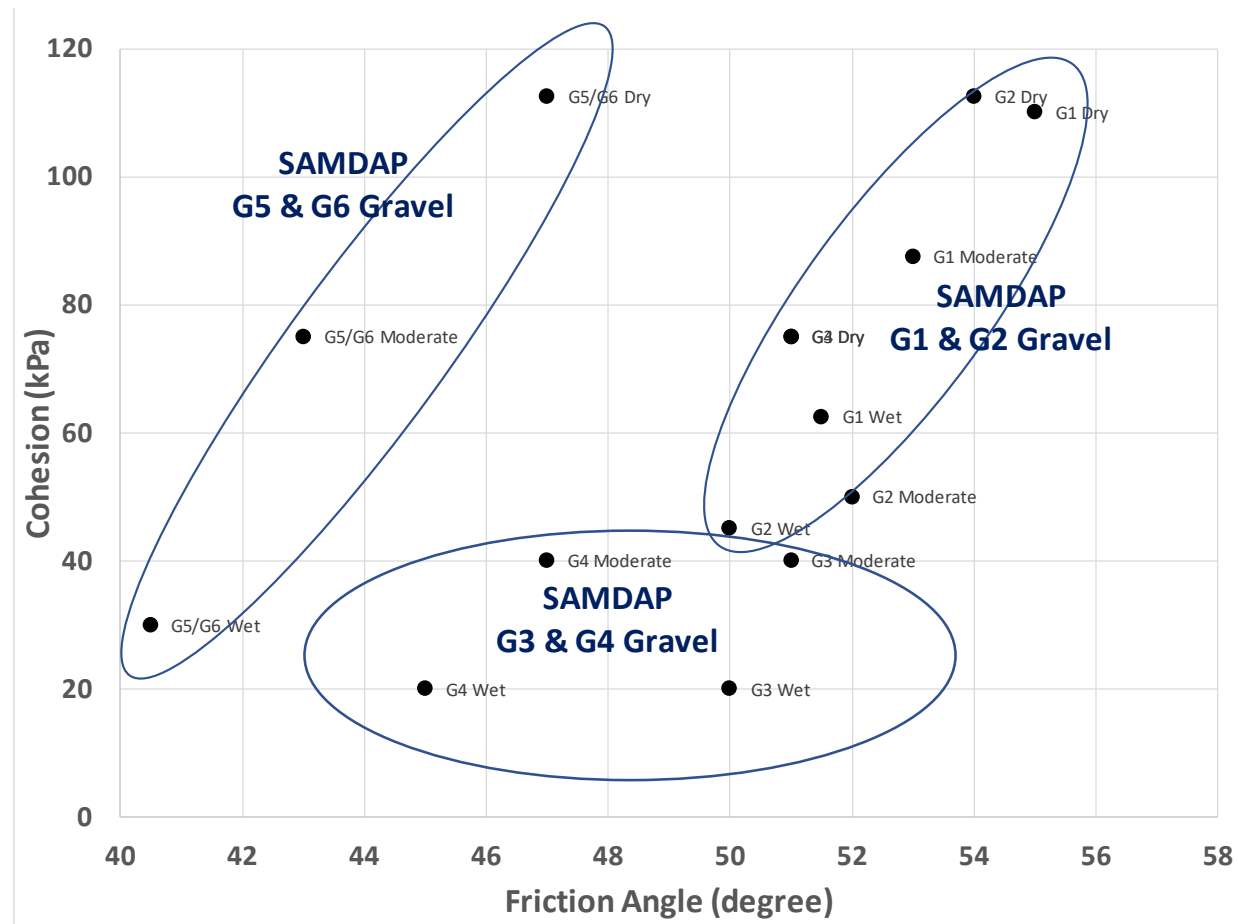


Figure 3.1: Typical friction angle and cohesion for each class of SAMDAP granular material

For a typical granular pavement configuration, the granular layer usually has a lower structural life than the subgrade layer, as shown in Figure 3.2. In other words, the granular layer is usually the critical layer which governs the structural life of the entire pavement. This is true as long as the granular pavement thickness is not excessively thin.

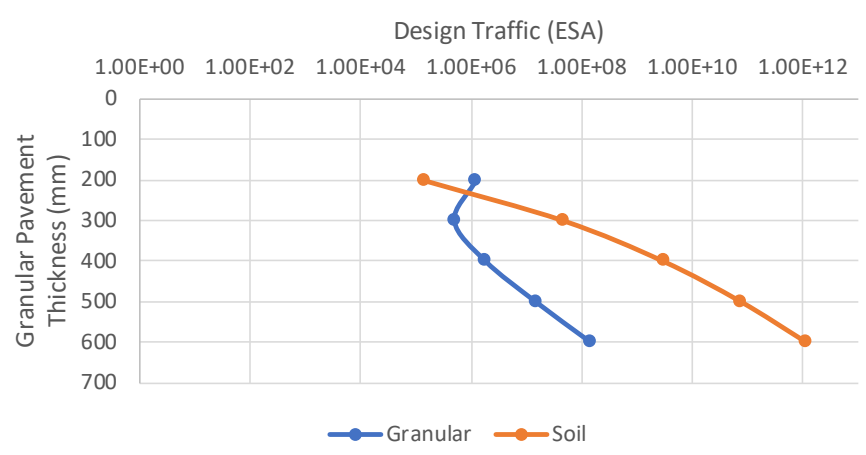


Figure 3.2: Structural life of granular and subgrade soil determined using the SAMDAP method over a subgrade CBR 10%

In contrast, the Austroads model was based on the empirical chart presented in (Austroads 2017): it represents the permanent deformation in all granular and subgrade layers. The relative contribution from the granular and subgrade layers is unknown.

When comparing the SAMDAP model with the Austroads model, more input parameters can be chosen in the SAMDAP model. The SAMDAP input parameters considered are summarised in Table 3.1. For illustrative purposes, it is assumed that only one granular material is used between the surface and the top of the subgrade.

Parameters	Values
Road category	A
	В
	С
	D
CBR	5%
	10%
	15%
	20%
Modulus of granular base	350 MPa
-	500 MPa
Moisture condition	normal
	moderate
	saturated

Table 3.1: Input parameters considered in the sensitivity analysis using the SAMDAP model

Similar to the Austroads empirical model, the granular thicknesses required for a given design traffic load depend on the subgrade CBR value as shown in Figure 3.3. However, it is noted that the subgrade CBR has a much lesser effect on the granular thickness in the SAMDAP model than in the Austroads model.

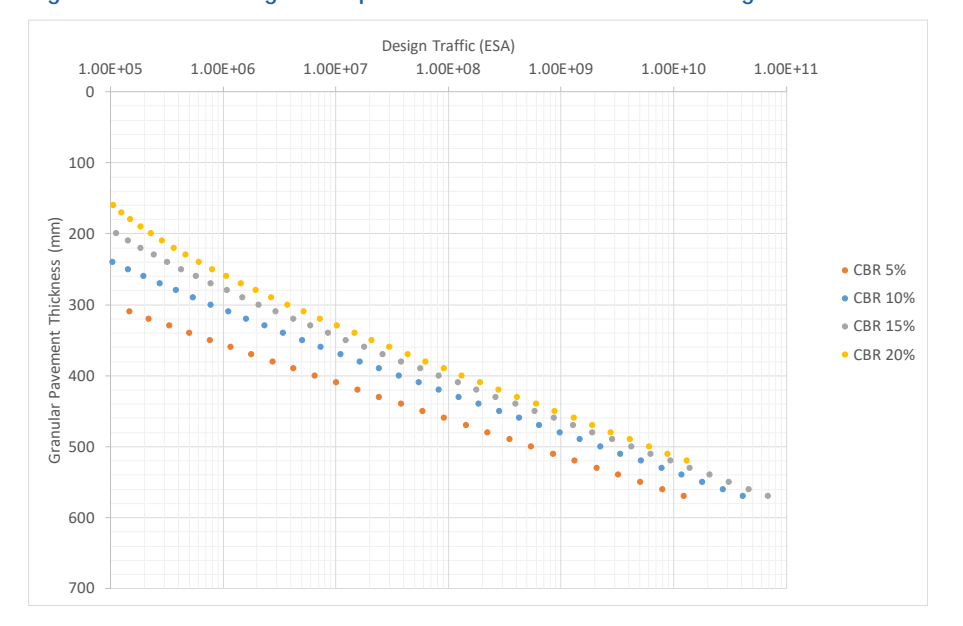


Figure 3.3: SAMDAP granular pavement thickness for different subgrade conditions

A sensitivity analysis of the different road category and drainage conditions is presented in Figure 3.4 and Figure 3.5. The higher the road category (i.e. Category A is a higher-class road than Category D), the higher the level of service that is required. Hence, a thicker granular pavement is needed as shown in Figure 3.4.

The long-term performance of the granular material also depends on the drainage condition (or more specifically the moisture content) of a road. Figure 3.5 confirms that a thicker granular pavement is required as the drainage condition degrades.

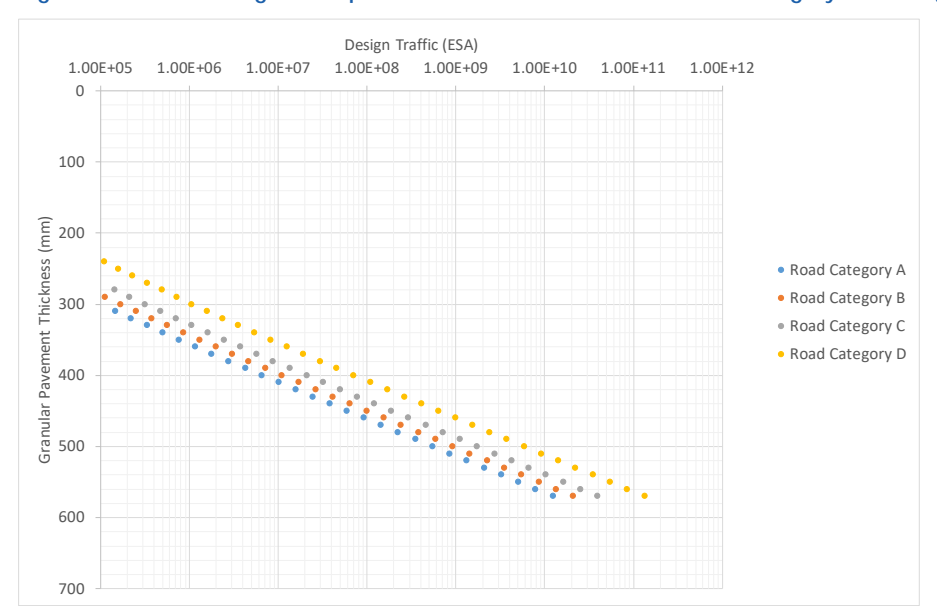
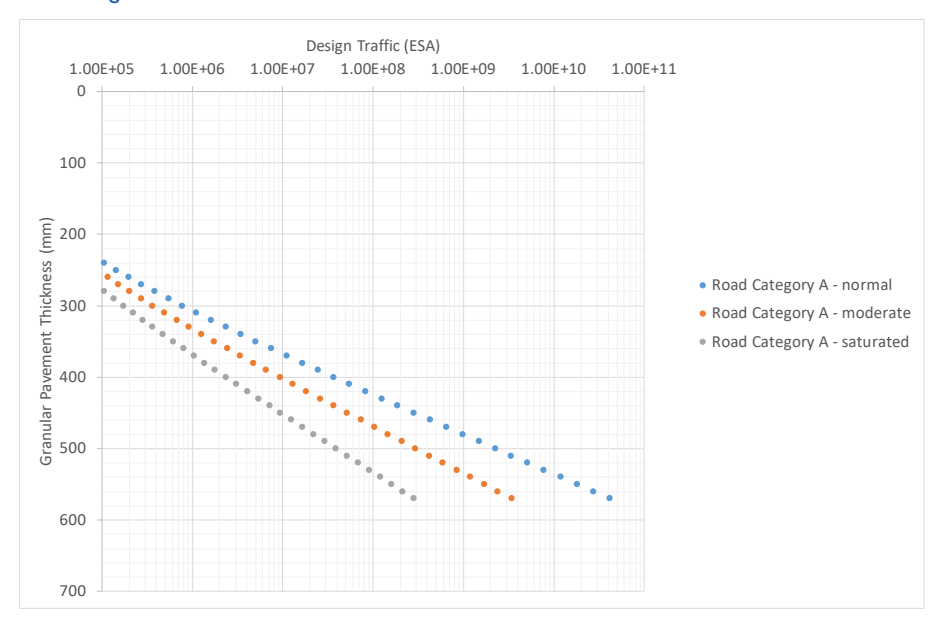


Figure 3.4: SAMDAP granular pavement thickness for different road category over subgrade CBR 5%

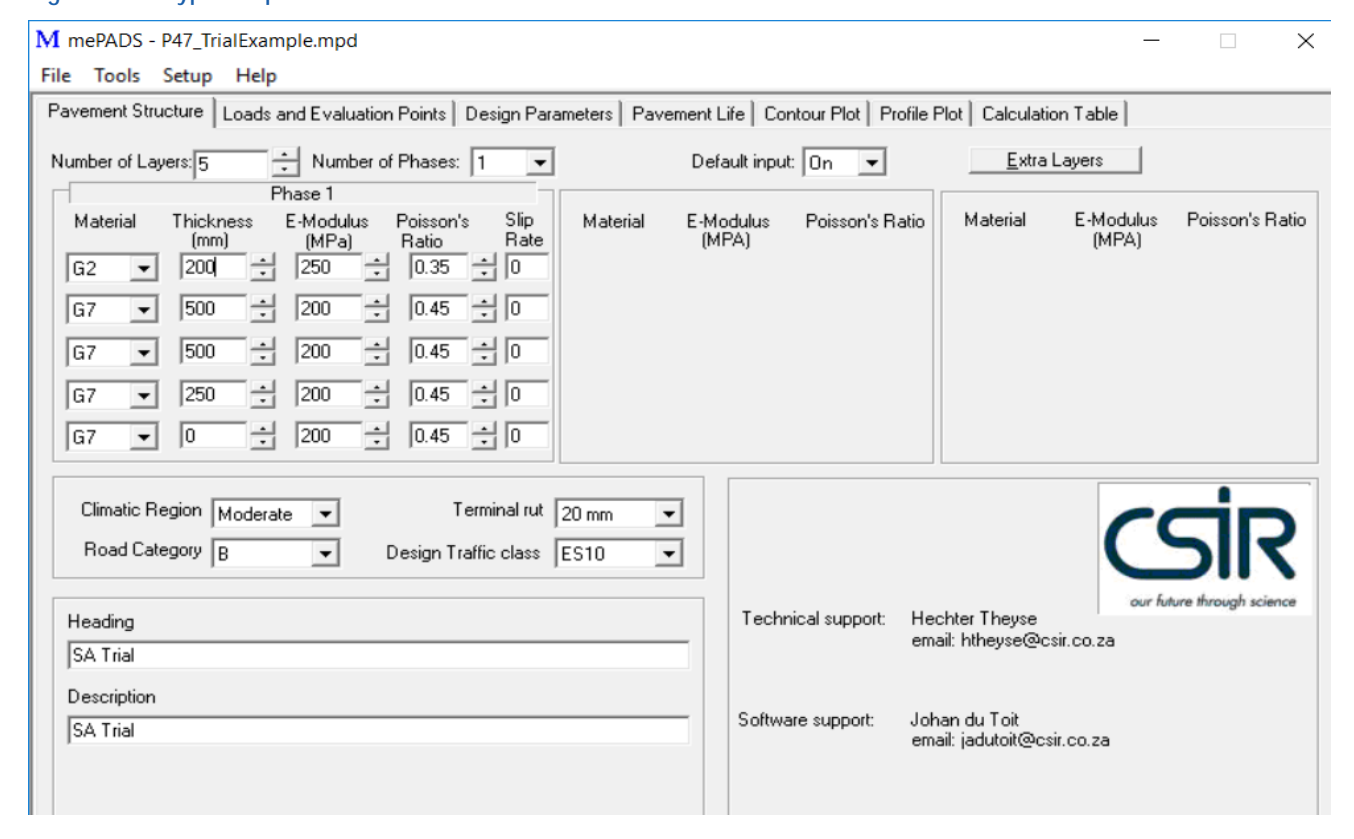
Figure 3.5: SAMDAP granular pavement thickness for different drainage conditions corresponding to category a road with subgrade CBR 10%



3.2 Design Examples using mePADS

Some design examples were carried out using the mePADS software, which adopts the SAMDAP approach. A typical screenshot of the input window software is shown in Figure 3.6.

Figure 3.6: Typical input window of mePADS software



A series of granular pavement types (G2 to G7) and granular layer thicknesses (300 – 600 mm) over different subgrade CBRs (5% to 20%) were analysed. A thickness design chart for a subgrade CBR of 5% is shown in Figure 3.7. It can be seen that, as the quality of granular material decreases (i.e. material quality decreases from G2 to G7), a thicker layer of granular material is required for the same subgrade CBR of 5%. The Figure also shows a line which represents the Austroads CBR 5% line from the empirical chart; it aligns closely with the G4 baseline.



Figure 3.7: mePADS design chart corresponding to SAMDAP granular pavement types with subgrade CBR 5%

The SAMDAP method was developed based on the shear strength of the granular material. Therefore, it is worthwhile to compare the shear strength parameters measured during this project for the local material representative in Queensland (refer Section 4.3) with some of the default values from the SAMDAP. This comparison is shown in Figure 3.8, with the material falling in the typical ranges for a SAMDAP G3 & G4 granular layer.

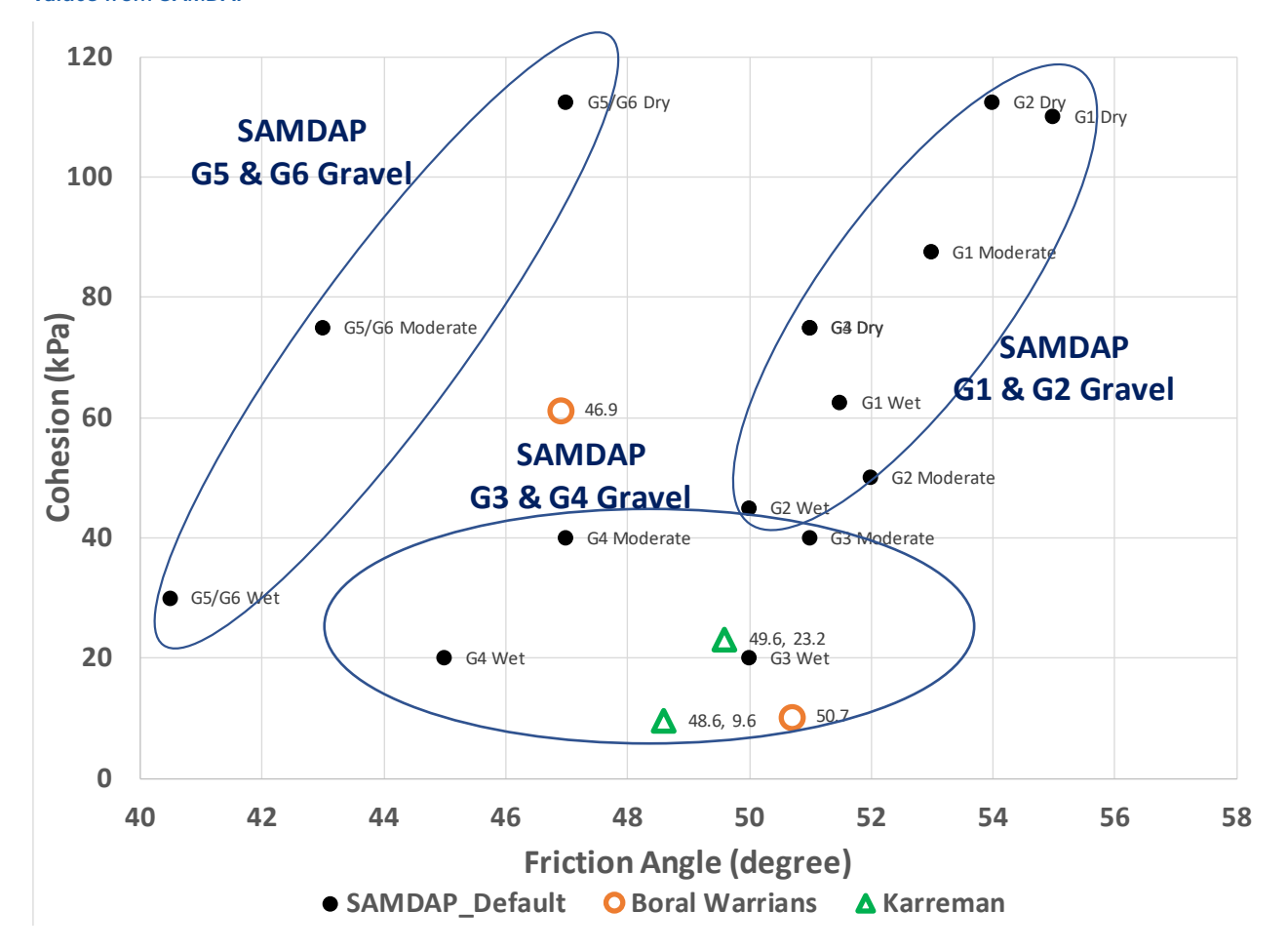


Figure 3.8: Comparison of friction angle and cohesion from the Boral Warrians and Karreman quarry against default values from SAMDAP

The other clear advantage of the SAMDAP system is that it incorporates fundamental soil material properties (such as friction angle and cohesion). This increases its flexibility to determine design solutions for a wider range of applications.

3.3 Summary

In this section, a review of the granular pavement design methodology, SAMDAP, has been presented. Based on the limited analysis undertaken, it is not possible to conclude whether the SAMDAP system is more or less conservative than the Austroads empirical design chart. The SAMDAP system incorporates many of the important factors (e.g. drainage condition, the degree of saturation, traffic intensity and subgrade strength) which affect the long-term performance of a granular pavement. More importantly, there is a clear advantage associated with using fundamental soil properties to increase the flexibility and reliability of design solutions.

The Austroads approach implicitly includes the permanent deformation contribution from all the granular and subgrade layers. This approach limits the pavement designer in terms of the ability to determine the critical layer within the pavement. Conversely, in the SAMDAP analysis, it is possible to determine which granular layer can be the critical layer that dictates the overall permanent deformation performance. Due to the limited access to premium-quality granular materials in Queensland, a more advanced model which embraces all types of granular materials is required to correlate laboratory and field permanent deformations with a higher degree of confidence. Future work can include using laboratory and field deformation results to compare performance with analytical models.

4 LABORATORY TESTING AND MODEL FITTING OF EXPERIMENTAL DATA

One of the tasks for this project was to characterise unbound granular materials that are representative of typical materials used in Queensland. Two crushed rock base quality materials were selected for the project, both Type 2.1 materials that meet the MRTS05 standard specification (TMR 2018a). The first material was sourced from the Boral Warrians quarry (about 450 km north-west of Brisbane), whilst the second material was sourced from the Karreman quarry near Mount Cotton (about 30 km south-west of Brisbane).

As explained in Section 1.2, the laboratory testing program was conducted in Year 1 of the project to meet the objective set out in the original project scope. The tests included petrographic analysis, grading, Atterberg limits, static triaxial test to determine the shear strength, as well as wheel tracking and resilient modulus tests to measure the plastic deformation of the different granular materials.

A summary of the test results is presented in this section of the report. It is noted that not all the test results were used in the revised scope of the project; however, it is possible that other projects may utilise this information in the future.

4.1 Petrographic Assessment

According to the petrographic reports, the aggregate from the Boral Warrians quarry was basalt, and the aggregate from the Karreman quarry was meta-greywacke. The main petrographic and geological assessment data is summarised in Table 4.1. Both samples qualified as appropriate road base material from the petrographic perspective.

Table 4.1: Petrographic assessment

Characteristics	Coarse (retained by 4.75 mm sieve)	Fine (passing 4.75 mm sieve)
Boral Warrians quarry		
General	Pyroxene BasaltFinely crystallinewith a tough sub-ophitic texture	
Alteration and weathering	Slightly weathered, showing oxidation of subtle, incipient weathering Lightly altered	of smectite clay which may be attributed to
Secondary minerals		Secondary mineral content is about 18% sostasis in interstitial spaces, altering glass
	 and along micro-fractures and rims of p As well as 1% idingsite and <1% calcite grains Lightly altered 	oyroxene and plagioclase e and sericite filling fractures in some felspar
Engineering assessment	 Hard Strong Pyroxene Basalt is predicted to be dura Suitable for use as a road base (supplied) 	
Karreman quarry		
General	Meta-greywackeCrystallineNon-porousSlightly foliatedveined	
Alteration and weathering	unweathered	
Secondary minerals	26% of weak, soft minerals 6% chlorite 13% sericite 6% mica 1% carbonaceous matter Carrying <1% pyrite	 35% of weak, soft minerals 9% chlorite 20% sericite 5% mica 1% carbonaceous matter
Engineering assessment	 Hard Strong Meta-greywacke is predicted to be dura Suitable for use as a road base (supplied) 	

4.2 General Material Characterisation Testing

Table 4.2 presents a brief summary of the material properties of the Boral Warrians and Karreman material. A comparison of the properties with the MRTS05 specification showed that both materials met the specification limits.

Table 4.2: Material characterisation data

Properties	MRTS 05 specification (Type 2.1) – Grading C	Boral Warrians	Karreman
	Grading (Q103A)		
Sieve sizes (mm)			
37.5	-	100	100
26.5	-	100	100
19.0	80 – 100	100	95
9.5	55 – 90	74	72
4.75	40 – 70	50	57
2.36	30 – 55	36	44
0.425	12 – 30	18	20
0.075	5 – 20	8.7	9.9
Fine ratio (Q103A)	0.3 -0.55	0.49	0.50
Crushed Particles	No limit	100	100
Flakiness Index (%)	Max 35	20	16
Atte	erberg limits (Q104A, Q105	and Q106)	
Linear shrinkage (%) Q106	≤ 3.5	0.4	1.8
Liquid limit (%)	≤ 25	21.6	19.2
Plastic limit (%)	n/a	19.4	16.4
Plasticity index (%)	≤ 6	2.2	2.8
Weighted Plasticity Index (%)	≤ 150	39	55
Weighted Linear Shrinkage (%)	≤ 85	7	35
	Apparent Particle Density	(Q109)	
Apparent Particle Density – Total (Q109A)	_	2.966	2.690
Apparent Particle Density – Fine Fraction (Q109A)	-	2.963	2.710
Apparent Particle Density – Coarse Fraction (Q109B)	-	2.968	2.676
Californian	Bearing ratio (Q113A) – sta	indard compaction	
CBR MDD (t/m³)	_	2.34	2.21
CBR OMC (%)	_	8.6	7.2
Preparation	-	Soaked	Soaked
CBR at 2.5 mm (%)	_	54	58
CBR at 5.0 mm (%)	_	104	98
Californian	Bearing ratio (Q113B) – mo	odified compaction	
CBR MDD (t/m³)	_	2.40	2.28
CBR OMC	-	5.8	5.2
Preparation	-	Soaked	Soaked
CBR at 2.5 mm	-	260	116
CBR at 5.0 mm	-	Exceeded CBR machine load cell range	210
Maximum dry density te	sting: standard and modifi	ed Proctor (Q142A and Q142	2B)
MDD _{std} (t/m³)	-	2.389	2.210
OMC _{std} (%)	-	7.5	7.2
MD _{mod} (t/m³)	_	2.419	2.309
OMC _{mod} (%)	_	6.8	5.3

Note 1: MRTS05 only refers to CBR values undertaken using the standard compaction effort as per (Q113A).

The particle size distribution (PSD) curves obtained for the two materials are presented in Figure 4.1. The grading curve of the Boral Warrians material is coarser compared with the Karreman material. Conversely, the Apparent Particle Density and the CBR values (at both compaction standards) of the Boral Warrians material are higher compared to the Karreman material.

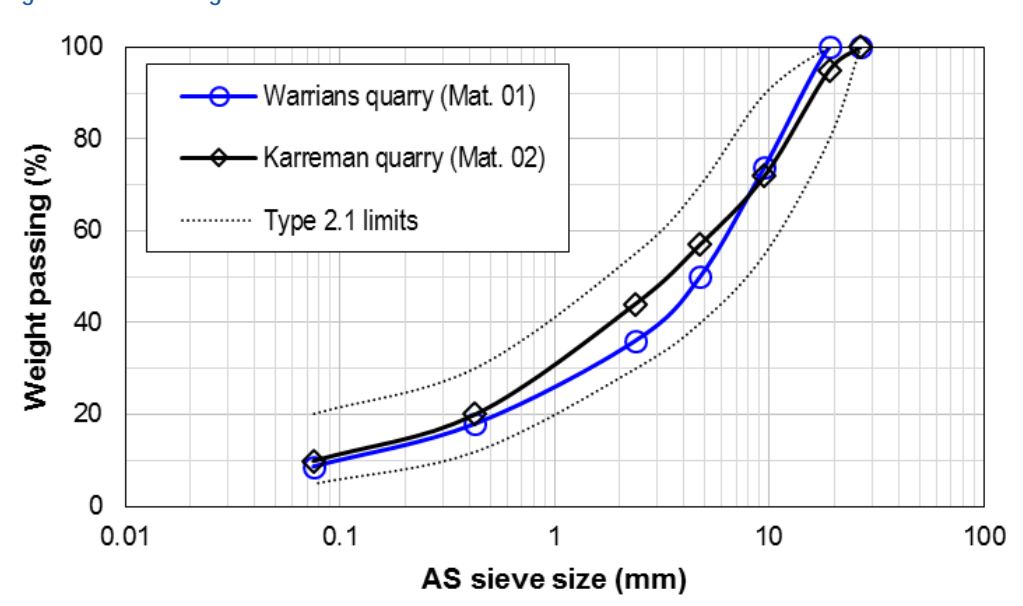


Figure 4.1: Grading curves

4.3 Static Shear Strength Testing

Four consolidated undrained (CU) triaxial tests, conducted in accordance with AS 1289.6.4.2, were carried out. Two specimens were obtained from the Boral Warrians Quarry, and two specimens from Karreman Quarry. The samples were compacted to 102% standard MDD and 98% modified MDD, and then tested at three effective confining pressure ranging from 50 to 200 kPa. Table 4.3 presents the results from the triaxial tests conducted on all four specimens.

Properties	Specimen 01 (Boral Warrians)	Specimen 02 (Boral Warrians)	Specimen 03 (Karreman)	Specimen 04 (Karreman)	
Cohesion, c' (kPa)	10.4	61.4	9.6	23.2	
Friction Angle,φ' (degree)	50.7	46.9	48.6	49.6	
Relative Compaction	102% Standard MDD	98% Modified MDD	102% Standard MDD	98% Modified MDD	
Dry Density (t/m³)	2.39	2.35	2.24	2.25	
Initial Moisture Content (%)	7.6	6.7	6.9	6.7	
Effective Confining Pressure (kPa)	46 – 197	52 – 201	52 – 203	43 – 195	

Table 4.3: Result of triaxial testing

4.4 Wheel-tracking Testing

Two sets of wheel-tracking tests were carried out in accordance with TMR test method Q149. The specimens were compacted into a slab at the target density and moisture content. The specimens were dried back to approximately 70% of OMC (degree of saturation of about 60 - 65%) before applying 5 000 load cycles (700 N load at 30 °C). The rut depth was measured, and the results reported at nominated cycles, as shown in Table 4.4.

It is noted that, as the moisture condition was higher than the field moisture condition, this result will have limited use when comparing with rutting measurement made in the field. Hence, the wheel-tracking information was not analysed further in this report.

Table 4.4: Results of wheel-tracking testing

	Sample ⁽¹⁾			Compaction	moisture saturation	Rut Depth (mm)					
Source		RDD	MDD	moisture content (%)		500 cycles	1000 cycles	2000 cycles	3000 cycles	4000 cycles	5000 cycles
Boral Warrians	BS16/044	102% Std.	2.389	7.3	99.7	0.53	0.55	0.56	0.56	0.57	0.57
Quarry		98% Mod.	2.419	6.8	80.3	0.57	0.60	0.61	0.62	0.63	0.63
Karreman Quarry	BS16/009	102% Std.	2.210	7.1	98.8	1.38	1.47	1.51	1.53	1.53	1.53
		98% Mod.	2.309	5.3	75.5	0.29	0.30	0.31	0.31	0.32	0.32

⁽¹⁾ Lab material register reference

4.5 RLT Test Results

4.5.1 Resilient Modulus (AGPT/T053)

The specimens were compacted at a moisture content close to the material OMC (Standard or Modified) and dried back to the test moisture content in a 40 °C oven.

The Main Roads Western Australia laboratory undertook the resilient modulus testing according to the Austroads test method AGPT/T053. The samples were compacted to the condition shown in Table 4.5. The test method provides material parameters k_1 , k_2 , and k_3 which can be used to characterise the resilient (recoverable) behaviour of the specimen. These parameters are commonly used as input to the Uzan model (Equation 5 in Section 2.1).

Table 4.5: Resilient modulus conditions

Source	Sample	Compaction method (Std./Mod.) (t/m³)	Target DD (t/m³)	Actual RDD (t/m³)	Compaction MC (%)	Test MC (%)	Test RMC (%)	Porosity	Degree of Saturation (DOS)	
Boral	BS16/044	Mod.	2.372	98	6.6	4.8	70.3	tbc	tbc	
Warrians Quarry			k1 = 366.6, k2 = 0.9163, k3 = -0.3219							
Quality		Std	2.434	101.9	7.4	5.3	70.2	tbc	tbc	
		k1 = 309.8, k2 = 0.6288, k3 = -0.1091								
Karreman	BS16/009	Mod.	2.268	98.2	5.1	3.7	70.2	tbc	tbc	
Quarry				k1 =	485.1, k2 = 0.80	62, k3 = -().3586			
		Std.	2.263	102.4	7.1	5.0	69.4	tbc	tbc	
				k1 =	224.0, k2 = 0.96	05, k3 = -0).3530			

4.5.2 RLT – Q137 Method (Permanent Deformation)

The RLT testing program covered a relatively large spectrum of preparation and testing conditions. The Standard and Modified compaction methods were used for the two materials targeting a range of relative compaction. The specimens were also compacted over a wide range of degree of saturation (DOS) levels. The testing matrix is summarised in Table 4.6.

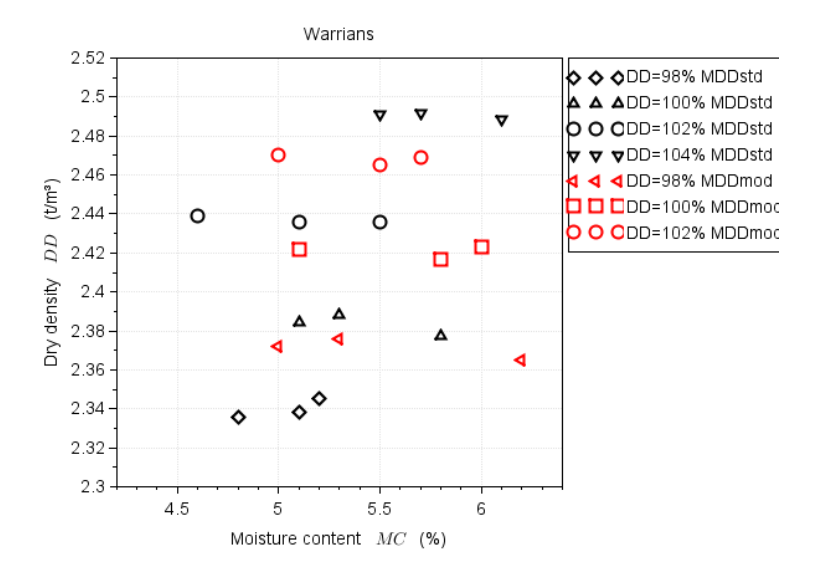
Table 4.6: Specimen preparation and testing conditions

	Relative Compaction									
Material	98% MDD _{STD}	100% MDD _{STD}	102% MDD _{STD}	104% MDD _{STD}	98% MDD _{MOD}	100% MDD _{мор}	102% MDD _{MOD}			
Boral Warrians	DOS 53 –	DOS 62 –	DOS 63 –	DOS 86 –	DOS 59 –	DOS 67 –	DOS 74 –			
	58%	69%	75%	94%	72%	79%	84%			
Karreman	DOS 56 –	DOS 55 –	DOS 53 –	DOS 60 –	DOS 61 –	DOS 61 –	DOS 79 –			
	65%	66%	65%	76%	82%	90%	99%			

For the Boral Warrians material, the dry density and porosity for each different compaction energy and moisture content are shown in Figure 4.2 and Figure 4.3, respectively. The dry density and porosity values were similar for specimens compacted at 102% standard Proctor compaction and 100% modified Proctor compaction. Also, the results were similar for 104% standard Proctor compaction and 102% modified Proctor compaction, and 100% standard Proctor compaction and 98% modified Proctor compaction.

The Boral Warrians data showed that the same dry density was achieved with a Standard compaction level that was approximately 2% higher than the nominal Modified compaction level.

Figure 4.2: Dry density and moisture content conditions (Type 2.1 base material from Boral Warrians quarry)



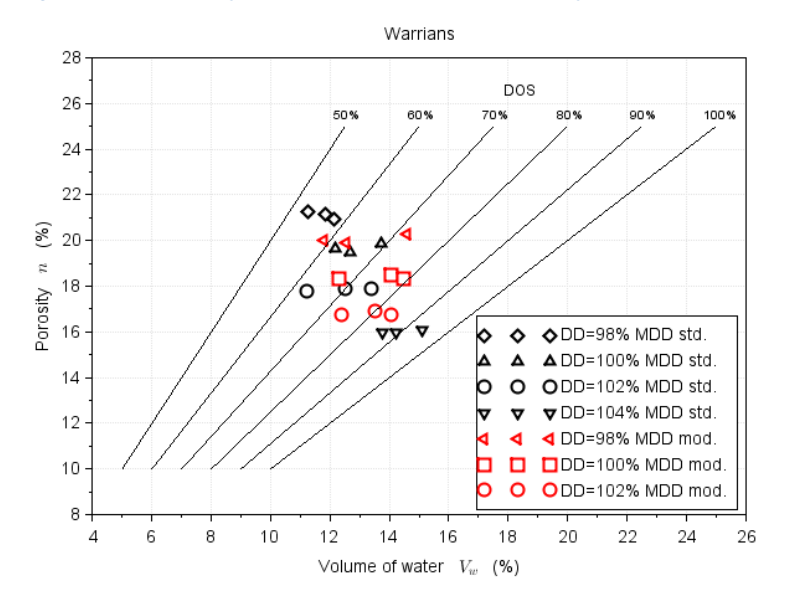


Figure 4.3: Porosity and water volume conditions (Type 2.1 base material from Boral Warrians quarry)

Similar plots of dry density and porosity are shown in Figure 4.4 and Figure 4.5 for the Karreman material. The results were similar for 104% Standard Proctor compaction and 100% Modified Proctor compaction as well as for 102% Standard Proctor compaction and 98% Modified Proctor compaction.

The Karreman data shows that the same dry density was achieved with a Standard compaction level that was approximately 4% higher than the nominal Modified compaction level. It is clear that the equivalency between the Standard and Modified Proctor compaction is dependent on the type of material.

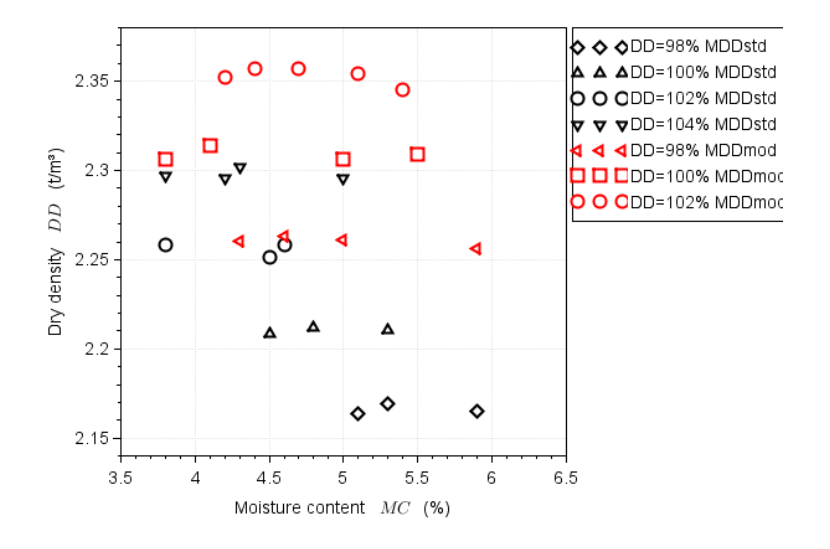


Figure 4.4: Dry density and moisture content conditions (Type 2.1 base material from Karreman quarry)

March 2019

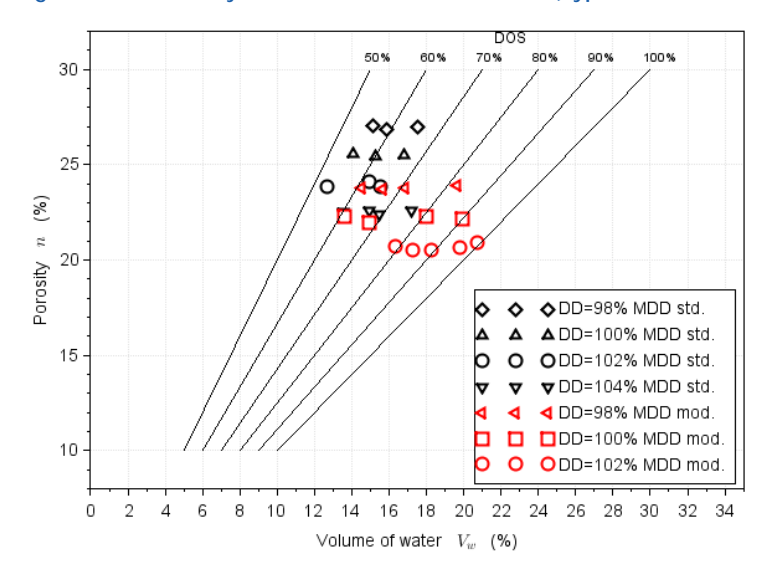


Figure 4.5: Porosity and water volume conditions (Type 2.1 base material from the Karreman quarry)

While a large number of RLT tests were conducted using the Standard and Modified compaction methods at different compaction levels, it is not part of this project to compare/correlate the difference in performance between different compaction standards.

4.5.3 Model fitting using RLT data – Boral Warrians Quarry

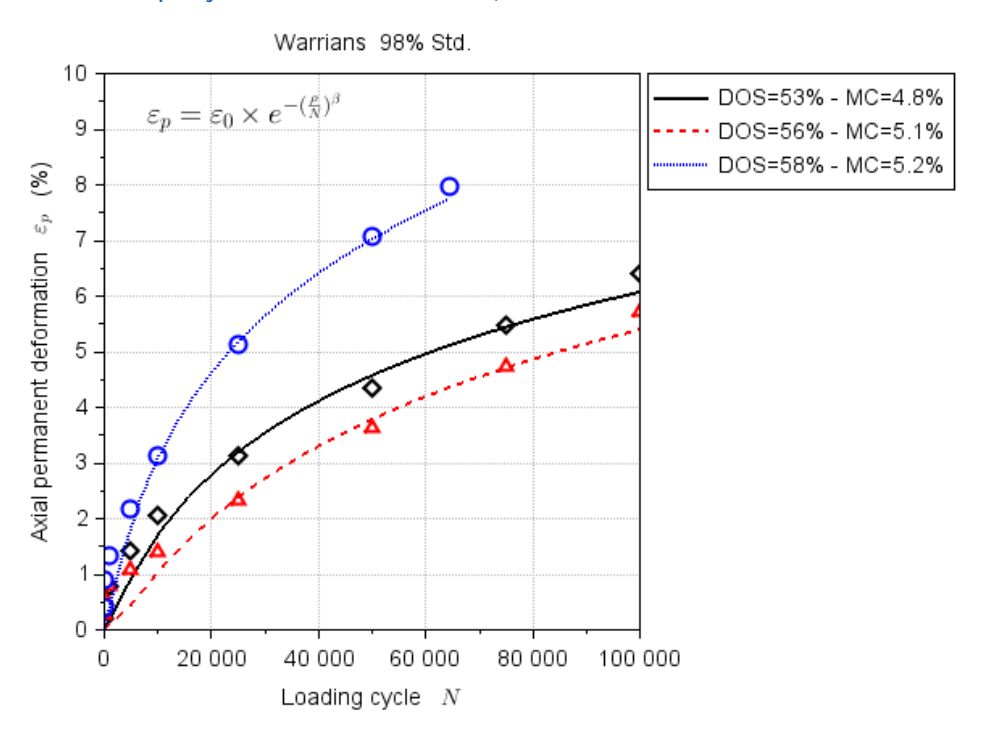
For RLT testing, the material was prepared at different densities and different moisture contents as summarised in Table 4.7. As discussed earlier in Section 2.3, in order to interpret the RLT data using the Tseng and Lytton model, a curve-fitting process is needed to determine the necessary model material parameters (ε_0 , ρ , β). An iterative algorithm was used to arrive at a set of best-fit material parameters (ε_0 , ρ , β) to the measured RLT data. For each compaction effort, moisture content, and density values, a set of material parameters were determined. Using these curves, the plastic deformation of the granular material can be computed using Equation 11. A full list of the material parameters and the corresponding coefficients of determination (R²) can be found in Appendix B

Figure 4.6 to Figure 4.9 shows the effect of the degree of saturation (moisture content) on the permanent axial deformation of the specimens. In each Figure, the markers denote the experimental data and the curved lines show the fitted model functions.

Table 4.7: Summary of the relative dry density, moisture content and degree of saturation of prepared RLT samples

Source	Energy	RDD	Moisture Content (%)	DOS
Boral Warrians Quarry	Standard	98%	4.8%	53%
			5.1%	56%
			5.2%	58%
		100%	5.1%	62%
			5.3%	65%
			5.8%	69%
		102%	5.5%	63%
			5.7%	70%
			6.1%	75%
	Modified	98%	5.0%	59%
			5.3%	63%
			6.2%	72%
		100%	5.1%	67%
			5.8%	76%
			6.0%	79%
		102%	5.0%	74%
			5.5%	80%
			5.7%	84%

Figure 4.6: RLT axial permanent deformation vs number of loading cycles (Boral Warrians quarry material DD = 98% MDD_{std.})



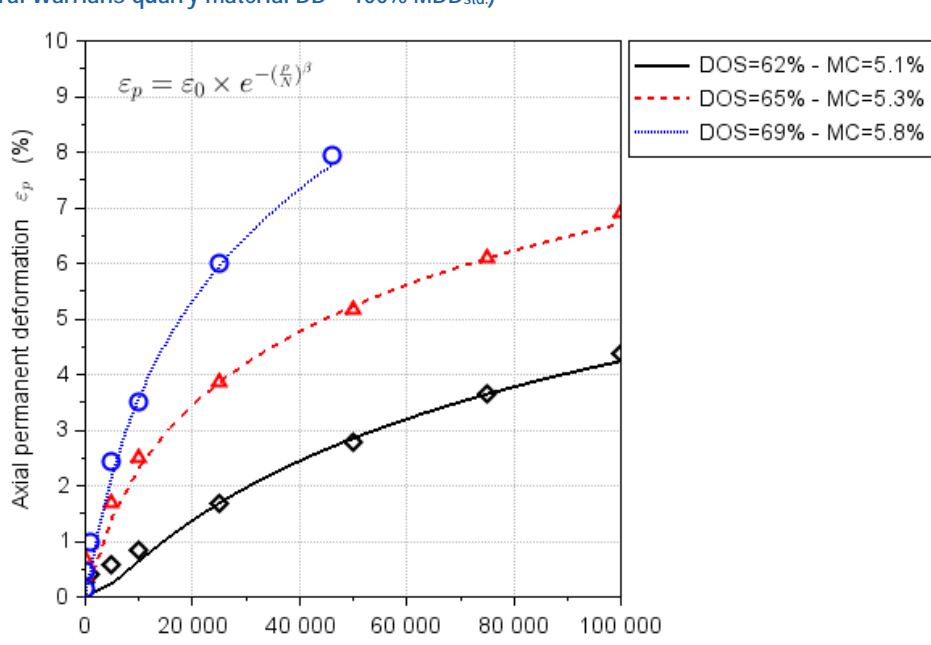
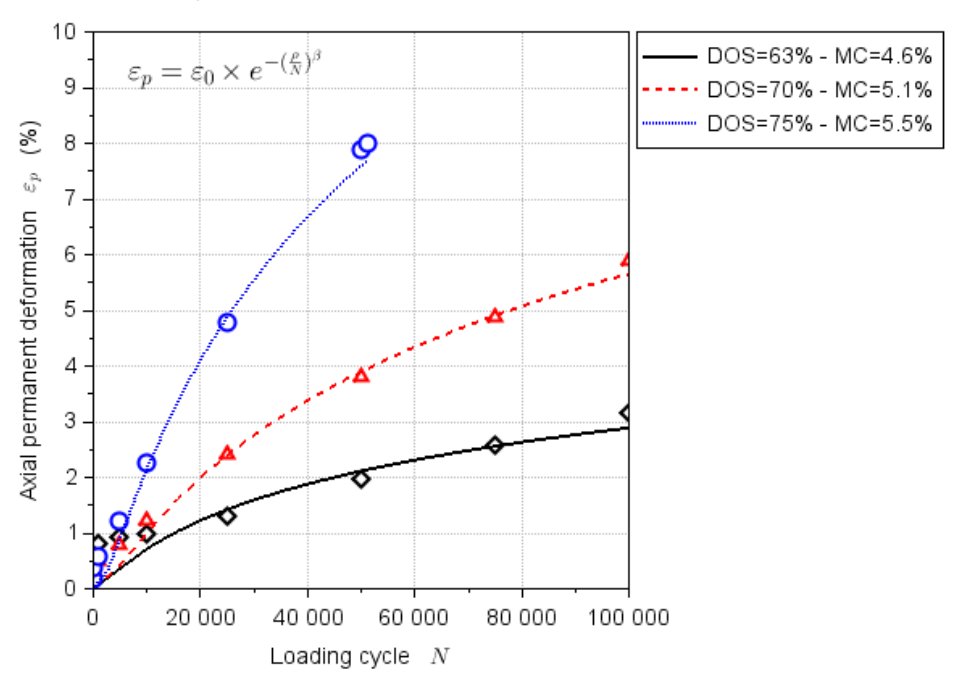


Figure 4.7: RLT axial permanent deformation vs number of loading cycles (Boral Warrians quarry material DD = 100% MDD_{std.})

Figure 4.8: RLT axial permanent deformation vs number of loading cycles (Boral Warrians quarry material DD = 102% MDD_{std.})

Loading cycle N



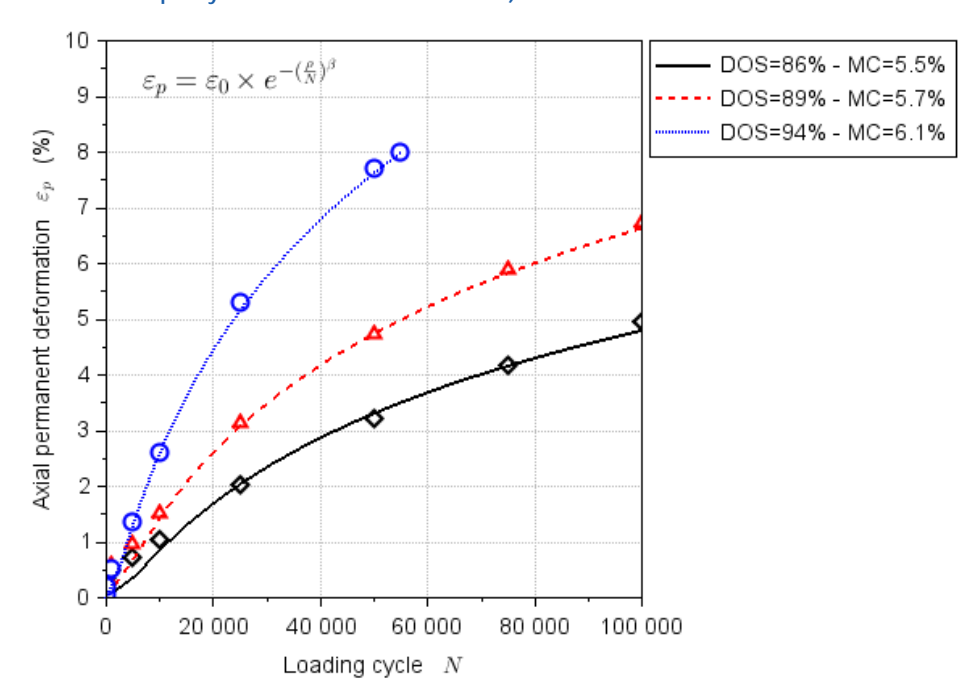


Figure 4.9: RLT axial permanent deformation vs number of loading cycles (Boral Warrians quarry material DD = 104% MDD_{std.})

4.5.4 Modelling Fitting RLT data – Karreman Quarry Material

For the RLT testing, the material was prepared at different densities and different moisture contents as summarised in Table 4.8. As discussed earlier in Section 2.3, in order to interpret the RLT data using the Tseng and Lytton model, a curve-fitting process was needed to determine the necessary model material parameters (ε_0 , ρ , β). An iterative algorithm was used to arrive at a set of best-fit material parameters (ε_0 , ρ , β) to the measured RLT data. For each compaction effort, moisture content, and density values, a set of material parameters were determined. Using these curves, the plastic deformation of the granular material was computed using Equation 11. A full list of the material parameters and the corresponding coefficient of determination (R²) values can be found in Appendix B.

Figure 4.10 to Figure 4.13 show the effect of the degree of saturation (moisture content) on the permanent axial deformation of the specimens. In each Figure, the markers denote the experimental data and the curved lines show the fitted model functions.

Table 4.8: Summary of the relative dry density, moisture content and degree of saturation of RLT samples

Source	Energy	RDD	Moisture Content (%)	DOS
Karreman Quarry	Standard	98%	5.1%	56%
			5.3%	59%
			5.9%	65%
		100%	4.5%	55%
			4.8%	60%
			5.3%	65%
		102%	3.8%	53%
			4.5%	62%
			4.6%	65%
		104%	3.8%	60%
			4.2%	65%
			4.3%	69%
			5.0%	76%
	Modified	98%	4.3%	61%
			4.6%	66%
			5.0%	71%
			5.9%	82%
		100%	3.8%	61%
			4.1%	68%
			5.0%	81%
			5.5%	90%
		102%	4.2%	79%
			4.4%	84%
			4.7%	89%
			5.1%	96%
			5.4%	99%

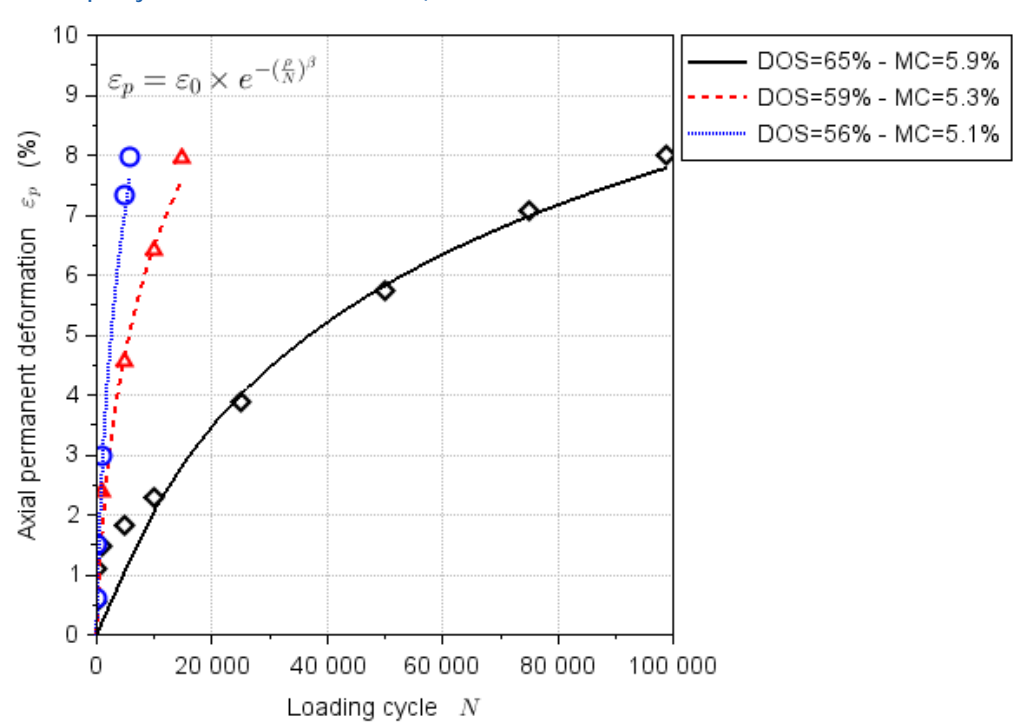
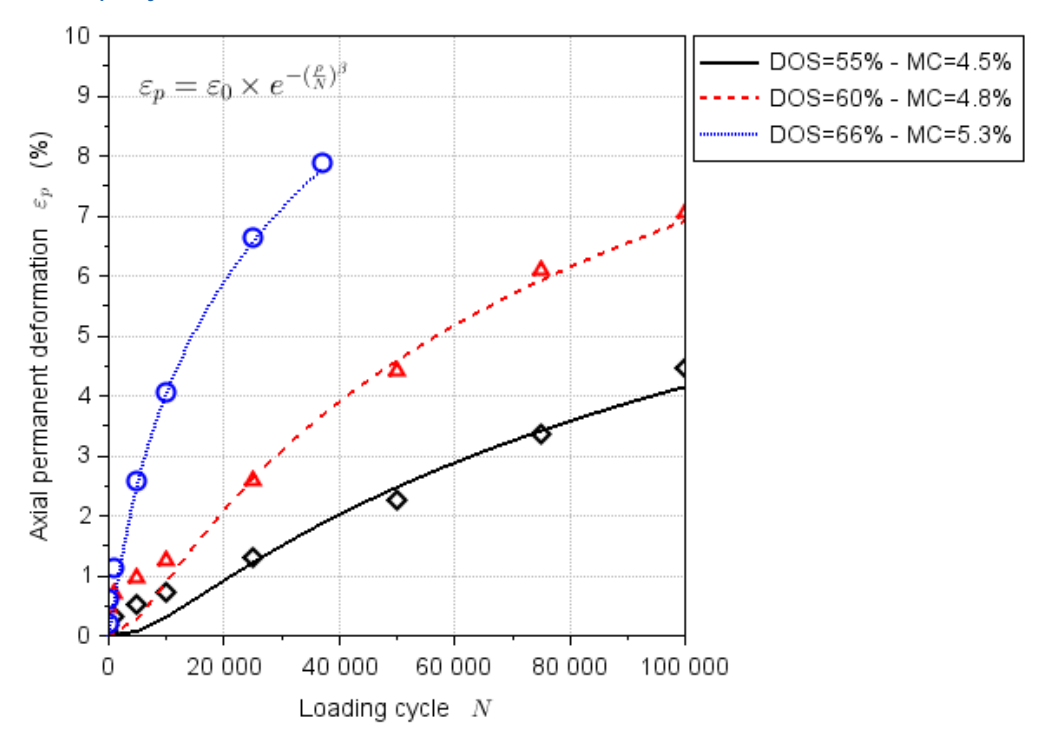


Figure 4.10: RLT axial permanent deformation vs the number of loading cycles (Karreman quarry material DD = 98% MDD_{std.})

Figure 4.11: RLT axial permanent deformation vs the number of loading cycles (Karreman quarry material DD = 100% MDD_{std.})



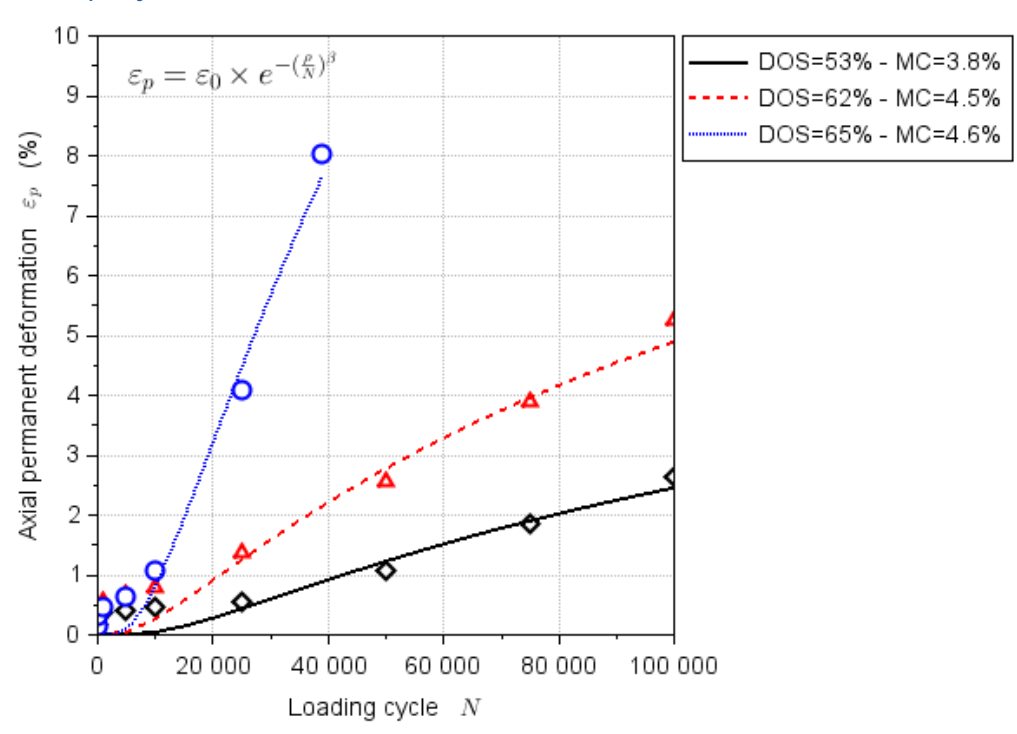
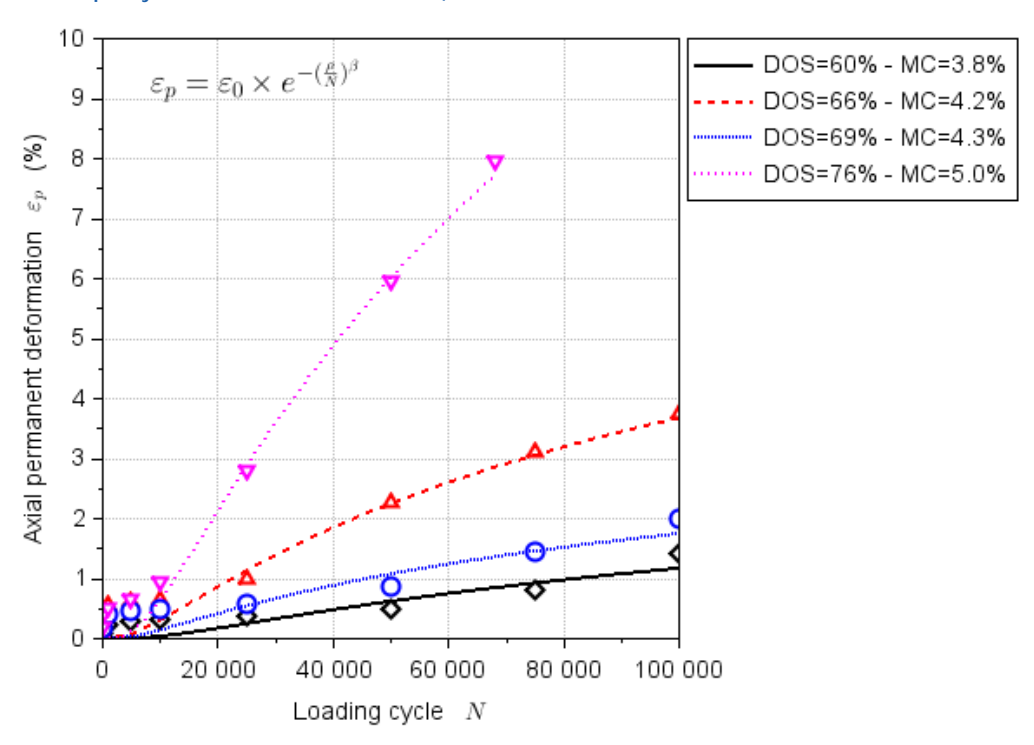


Figure 4.12: RLT axial permanent deformation vs the number of loading cycles (Karreman quarry material DD = 102% MDD_{std}.)

Figure 4.13: RLT axial permanent deformation vs the number of loading cycles (Karreman quarry material DD = 104% MDD_{std.})



Overall, the Tseng and Lytton model provided a mathematical equation which was successfully fitted to the permanent strain data measured in the laboratory. Despite providing a good agreement, the model was not well suited when the deformation strain rate increased (Range C, as discussed in Section 2.2). For conditions that fall into Range C (incremental collapse stage), material models other than that proposed by Tseng and Lytton will be needed.

5 **COMPARISON OF RLT DATA WITH FIELD MEASUREMENTS**

In the previous section, the RLT data collected in the laboratory testing program was used to determine the material parameters needed to fit the Tseng and Lytton model. This was accomplished by using an iterative curve-fitting technique.

This section summarises the results of inputting these material parameters into the plastic strain model (Tseng and Lytton) to predict permanent deformation. The predicted deformation was then compared with field performance data collected on a recent project along a section of the Centenary Highway. Refer to the NACoE P47 final report (Lee, Griffin & Conaghan 2018) for a more detailed discussion of the Centenary Highway project.

The predicted and observed pavement performance was compared based on the Karreman Type 2.1 material. This was because the material used in the Centenary Highway works was sourced from Karreman guarry at Mt Cotton and, although it was classified as a High Standard Granular (HSG) material, it was very similar to the Type 2.1 material. The respective material properties are shown in Table 5.1.

Only a preliminary analysis was undertaken to gauge the feasibility of adopting the Tseng and Lytton model to predict field condition. The analysis can only be treated as a preliminary for the following reasons:

- Laboratory testing was only performed on the Type 2.1 base layer. It was assumed that all of the deformation occurred in the granular base layer, which is not necessarily true depending on the stress condition in the subbase and subgrade layers.
- The RLT data available was not representative of the field density and moisture conditions before the Centenary Highway was sealed. For accurate prediction, the RLT data should be collected at the condition that closely simulates the field condition.

Table 5.1: Material properties of Karreman Type 2.1 and quarry samples for Centenary Highway

Material properties	Karreman Type 2.1	Centenary Highway (HSG specification)
Liquid Limit	19.2	19
Plastic Limit	16.4	15
Plasticity Index	2.8	4
Weighted Plasticity Index	55	70
Weighted Linear Shrinkage	35	62
Linear Shrinkage	1.8	3
Flakiness Index	16	20
Crushed Particles	100	100
Weak Particles	0.3	
Apparent Particle Density (Fine)	2.69	
Apparent Particle Density (Coarse)	2.71	
Standard MDD	2.21	2.156
Standard OMC	7.2	6.8
Modified MDD	2.309	
Modified OMC	5.3	
CBR STD	98	
CBR MOD	210	
Petrographic	Greywacke	Greywacke
Wet 10% Fines Value (min.)	> 125	
Wet strength (kN)		179
Dry strength (kN)		227
Maximum wet/dry variation	< 35	22
Minimum degradation factor	> 45	52
PSD 37.5 mm	100	100
PSD 26.5 mm	100	100
PSD 19.0 mm	95	97
PSD 9.5 mm	72	74
PSD 4.75 mm	57	58
PSD 2.36 mm	44	41
PSD 425 μm	20	17
PSD 75 μm	9.9	10
Fines Ratio	0.3 - 0.55	0.48

A typical cross-section of the Centenary Highway project is as shown in Figure 5.1.

Page 35 TC-710-4-4-8

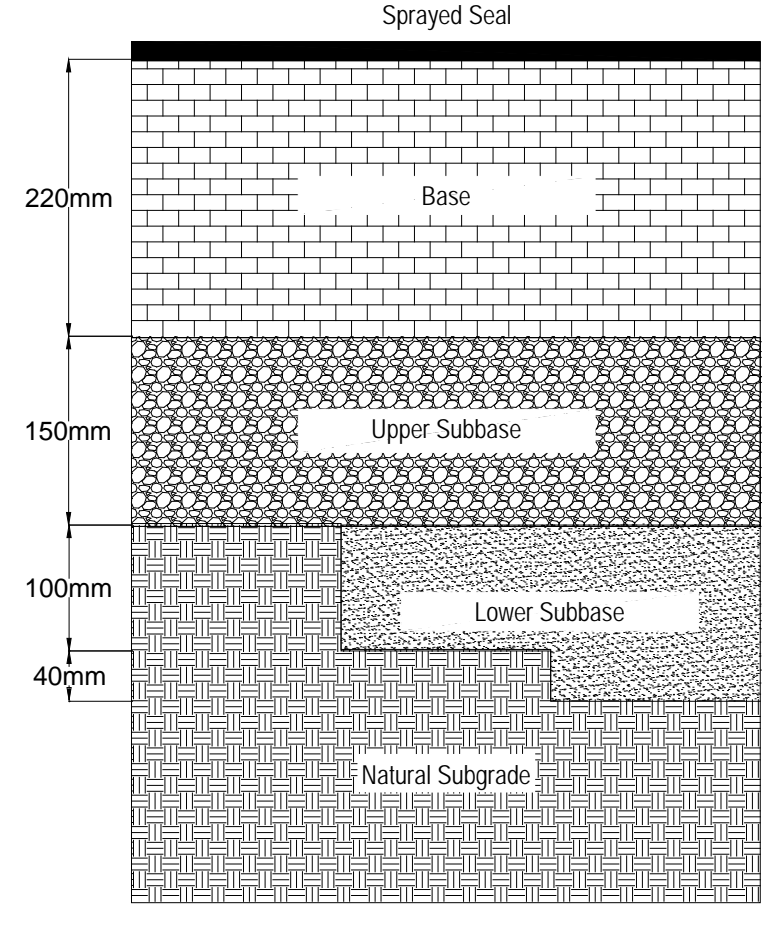


Figure 5.1: Trial pavement design cross-section depicting variable lower subbase thickness

5.1 Analysis Procedure

To compute the permanent deformation of the granular base layer, the following steps were undertaken:

- 1. Determine the Centenary Highway pavement profile (Figure 5.1) using the information obtained from construction records.
- 2. Determine the model material parameters to be used Select the parameters (Section 4.5.4) that are closest to the density and moisture condition in the field.
- 3. Determine the vertical compressive strain profile (Section 5.1.1).
- 4. Compute the permanent deformation and compare against the field measured data (Section 5.1.2).

5.1.1 Vertical Strain-Profile

For the Tseng and Lytton model to predict the plastic (or permanent) deformation of a granular layer, the vertical strain (\$\varepsilon zz\$) profile is required. Different analysis software can be used. In this study, CIRCLY (Wardle 1976) (a multi-layer linear elastic model) and APADS (Bodin et al. 2014) (a finite element model which incorporate both linear and non-linear granular model) were used. Five numerical analyses were undertaken with the material properties summarised in Table 5.2.

Table 5.2: Summary of material parameters adopted in the numerical analysis

Analysis	Type of Analysis	The degree of Anisotropy of all layers (Ev/Eh)	Granular Base – Ev (MPa)	Granular Subbase – Ev (MPa)	Subgrade – Ev (MPa)
CIRCLY E=350	MLEA	2.0	350	150	100
CIRCLY E=500	MLEA	2.0	500	150	100
APADS - M1	FEA – linear	2.0	350	150	100
APADS - M2	FEA – non-linear	2.0	RLT data (98% standard RDD & 70% OMC) – NOTE 1	150	100
APADS – M3	FEA – non-linear	2.0	RLT data (98% modified RDD & 70% OMC) – NOTE 1	150	100

MLEA = Multi-layer Linear Elastic Analysis.

FEA = Finite Element Analysis.

Note 1: This is the RLT data set that is closest to the field condition before sealing (average DOS 40%). However, it is noted that the field condition still has a much higher density and lower degree of saturation that the testing conditions of the RLT data.

Figure 5.2 shows the vertical strain profiles obtained from each analysis. As expected, the higher the assumed modulus, the lower the reported vertical strain. The strain profile generated from the CIRCLY analysis (E=350~MPa) was the highest, and the APADS software (with parameters obtained from the RLT results — corresponding to 98% Modified RDD & 70% OMC) being the lowest.

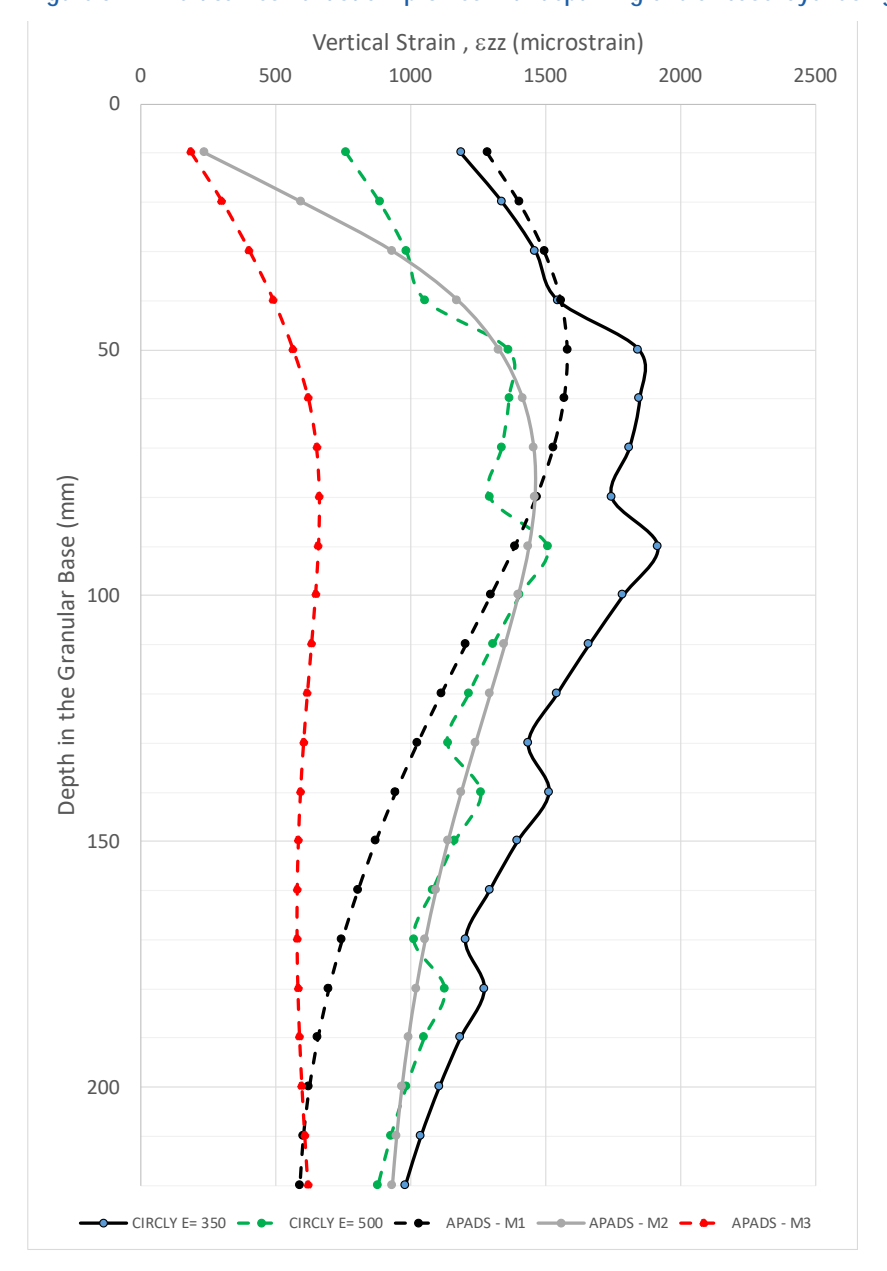


Figure 5.2: Vertical resilient strain profiles with depth in granular base layer using CIRCLY and APADS

5.1.2 Comparison of Computed and Measured Permanent Deformation

After obtaining the model material parameters and vertical strain profiles for the Centenary Highway, the permanent deformation was computed using the Tseng and Lytton model (Equation 11). For each of the assumed vertical strain profiles (i.e., M1, M2, M3), the computed permanent deformation was compared against the field condition data collected from the Centenary Highway over 36 months (Lee, Griffin & Conaghan 2018). The comparison is shown in Figure 5.3. The comparison indicates that the permanent field deformation compares well with the prediction calculated using the resilient strains obtained with the APADS-M3 model.

As shown in Figure 5.3, the permanent deformation predicted using the M3 vertical strain profile generally agrees with the field performance to date. The M3 vertical strain profile was developed using the material parameters developed from laboratory RLT data (98% Modified RDD & 70% OMC). The material in the field has a much higher density and lower degree of saturation (average DOS of around 40%) than the selected laboratory RLT data.

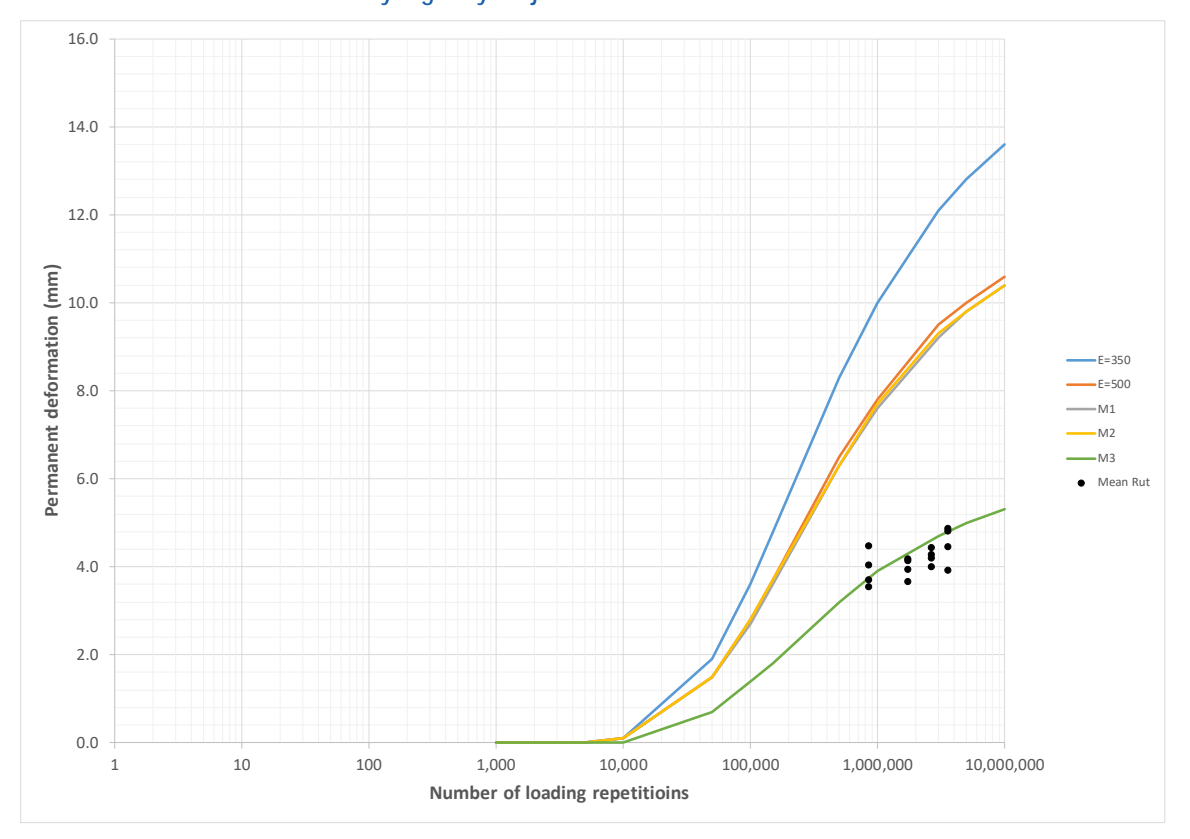


Figure 5.3: Comparison of predicted permanent deformation of granular base layer and the condition data measured in the first 36 months at the Centenary Highway Project

5.2 Summary

This section of the report has addressed the predicted permanent deformation based on some numerical analysis models (both linear and non-linear). The non-linear model appears to provide a vertical strain profile that gives the closest permanent field deformation measurement. It is noted that the moisture condition in the granular pavement is likely to be lower than the moisture condition tested in the RLT tests. Future work should include additional RLT testing at conditions that more closely match the field moisture conditions. The field data used in this study only represents the early life of the Centenary Highway; more data should be collected in the future as deterioration continues.

6 SUMMARY AND FUTURE RESEARCH PLAN

6.1 Summary

Unbound granular pavements fail after excessive permanent deformation accumulates in the wheel path. Currently, there is no established Australian performance model to predict and limit the permanent deformation of unbound granular layers. This report presents the findings from NACOE Project P47, the aim of which was to improve the modeling and prediction of the permanent deformation in unbound granular pavement layers. The report covers Year 1 and Year 2 of the research work. The project involved extensive laboratory testing of the unbound granular material. The data was then used to obtain fitted model parameters based on the Tseng and Lytton model. The deformations predicted using the Tseng and Lytton model were then compared with the limited field data available from a granular pavement located in south-east Queensland. It is concluded that the Tseng and Lytton model (adopted by the US in the MEPDG) was successful in fitting the permanent strain data measured in the laboratory. It was also found that there was a reasonable fit between the predicted permanent deformation and the mean rut depth measured in a field trial site.

The study also included a sensitivity analysis of the South African Mechanistic Design Analysis Procedure (SAMDAP). Different input parameters were used to predict the required granular pavement thickness to limit the plastic deformation within the granular layer. Based on the limited analysis that was undertaken, it was not possible to conclude whether the SAMDAP system was more or less conservative than the Austroads empirical design chart. Nevertheless, the approach of considering the permanent deformation from within the granular layer is in line with the MEPDG approach taken in the USA.

While the project to date has not led to the development of an advanced performance model for unbound pavements, work has been conducted to explore the potential suitability of adopting an alternative and currently-available performance model instead of the current Austroads approach.

6.2 Future Research

Future research into the adoption of an advanced performance model for unbound granular pavement materials may include the following:

- Resilient modulus testing conducted in accordance with the TMR standard test method (Q137) only tests the materials under one confining pressure (σ3 = 750 kPa). This prevents the test results being used to study the effect of confining pressure on the granular material. A more comprehensive approach is recommended as given in Austroads Test Method AG: PT/T053 Determination of permanent deformation and resilient modulus characteristics of unbound granular materials under drained conditions.
- Overseas approaches (e.g. South Africa) report different permanent deformations from different granular and underlying subgrade layer. In the current Australian practice, it is not clear what the relative contributing proportion from the granular and subgrade layer are. This requires further investigation, including the installing multi-depth deformation gauges in trial pavements to determine the vertical deformation profile throughout the granular and subgrade zone.
- Recent Austroads research (Austroads 2017) concluded that the large-scale wheel-tracking test was the best available test to rank granular base rut-resistance. This test should be considered in any future aspects of this study.
- The current model investigation (Tseng & Lytton 1989) is not adequate in terms of its ability to predict the later stage of the permanent deformation in the granular material.
- The permanent deformation predicted using the Tseng and Lytton model (using Karreman Type 2.1 material) was compared with the field performance on the Centenary Highway,

which comprises high standard granular (HSG) material from the same quarry. More pavement trials and/or APT testing is needed across Queensland to validate the field performance aspect of this project.

TC-710-4-4-8 Page 41 March 2019

REFERENCES

- Ahmed, AW & Erlingsson, S 2013, 'Evaluation of permanent deformation models for unbound granular materials using accelerated pavement tests', Road Materials and Pavement Design, vol. 14, no. 1, pp. pp 178-95, doi,
 - http://dx.doi.org/10.1080/14680629.2012.755936

http://www.tandfonline.com/doi/abs/10.1080/14680629.2012.755936 https://trid.trb.org/view/1244600>.

- Araya, AA 2011, 'Characterization of Unbound Granular Materials for Pavements', Design and Construction, Delft University of Technology.
- Austroads 2017, Guide to pavement technology: part 2: pavement structural design, AGPT02-17, Austroads, Sydney, New South Wales, Australia.
- Ba, M, Tinjum, JM & Fall, M 2015, 'Prediction of permanent deformation model parameters of unbound base course aggregates under repeated loading', Road Materials and Pavement Design, vol. 16, no. 4, pp. pp 854-69, doi, http://dx.doi.org/10.1080/14680629.2015.1063534 https://trid.trb.org/view/1375554>.
- Bodin, D, Gonzalez, A, Jameson, G, Moffatt, M & Oeser, M 2014, 'APADS: finite method software for enhanced pavement analysis including nonlinear behavior of granular materials'.
- Erlingsson, S, Rahman, S & Salour, F 2017, 'Characteristic of unbound granular materials and subgrades based on multi stage RLT testing', Transportation Geotechnics, vol. 13, no., pp. 28-42, doi: https://doi.org/10.1016/j.trgeo.2017.08.009, http://www.sciencedirect.com/science/article/pii/S2214391217300399>.
- Lee, J, Griffin, J & Conaghan, A 2018, P15 Queensland Trial of High Standard Granular Base Track Star Alliance Project (Year 4 - 2016/17), report P15, National Asset Centre of Excellence (NACOE), Brisbane, viewed 28/05/2018, http://nacoe.com.au/wp- content/uploads/2018/03/PRP16023 P15 QLD-Trial-of-High-Standard-Granular-Base-TrackStrar-Alliance-Project_Final.pdf>.
- Lekarp, F, Dawson, A & Elsevier 1998, 'MODELLING PERMANENT DEFORMATION BEHAVIOUR OF UNBOUND GRANULAR MATERIALS', Construction and Building Materials, vol. 12, no. 1, pp. p. 9-18, doi, https://trid.trb.org/view/487348>.
- Rahman, MS & Erlingsson, S 2016, 'Modelling the Moisture Dependent Permanent Deformation Behavior of Unbound Granular Materials', The 3rd International Conference on Transportation Geotechnics, Guimarães, Portugal, Elsevier B.V., vol. 143, pp. 921-8.
- Siripun, K, Jitsangiam, P & Nikraz, H 2012, 'The design model of unbound granular materials for flexible pavement', Australian Journal of Civil Engineering, vol. 10, no. 1, pp. 1-9, doi: https://doi.org/10.7158/14488353.2012.11463970.
- Theyse, H & Kannemeyer, L 2010, 'New directions in the design of unbound granular layers in road pavements', Civil Engineering = Siviele Ingenieurswese, vol. 2010, no. v18i8, doi, http://journals.co.za/content/civeng/18/8/EJC26410.
- Theyse, HL, De Beer, M, Rust, FC & Transportation Research, B 1996, 'OVERVIEW OF SOUTH AFRICAN MECHANISTIC PAVEMENT DESIGN METHOD', Transportation Research Record, vol., no. 1539, pp. p. 6-17, doi, http://dx.doi.org/10.3141/1539-02

https://trid.trb.org/view/469388>.

- Theyse, HL, Legge, FTH, Pretorius, PC & Wolff, H 2007, 'A Yield Strength Model for Partially Saturated Unbound Granular Material', *Road Materials and Pavement Design*, vol. 8, no. 3, pp. pp 423-48, doi, https://trid.trb.org/view/836838>.
- Tseng, KH & Lytton, RL 1989, 'Prediction of Permanent Deformation in Flexible Pavement Materials', Implication of Aggregates in the Design, Construction, and Performance of Flexible Pavements, ASTM International.
- Wardle, LJ 1976, Program CIRCLY: a computer program for the analysis of multiple complex circular loads on layered anisotropic media user's manual, report, viewed, https://trid.trb.org/view/1207683>.

Australian Standards

AS 1289.6.4.2:2016, Methods of testing soils for engineering purposes: Soil strength and consolidation tests – Determination of compressive strength of a soil – Compressive strength of a saturated specimen tested in undrained triaxial compression with measurement of pore water pressure.

TMR Test Methods

Q103A: Particle size distribution of soil – wet sieving, November 2018.

Q104A: Liquid limit of soil, November 2018.

Q105: Plastic limit and plasticity index of soil, November 2018.

Q106: Linear shrinkage of soil, November 2018.

Q109A: Apparent particle density of soil - fine fraction, September 2017.

Q109B: Apparent particle density of soil - coarse fraction, September 2017.

Q113B: California Bearing Ratio of soil – modified, November 2018.

Q137: Permanent deformation and resilient modulus of granular unbound material, November 2018.

Q142A: Dry density-moisture relationship of soils and crushed rock - standard, November 2018.

Q142B: Dry density-moisture relationship of soils and crushed rock – modified, November 2018.

Q149: Deformation of granular material – wheel tracker, November 2018.

Austroads Test Methods

Austroads test method AGPT/T053, Determination of permanent deformation and resilient modulus characteristics of unbound granular materials under drained conditions, September 2007.

APPENDIX A MATHEMATICAL MODELS ANALYTICS

A.1 Tseng and Lytton (1989)

$$\varepsilon_{p} = \varepsilon_{0} \times \exp\left(\left(\frac{\rho}{N}\right)^{\beta}\right)$$

$$\ln(\varepsilon_{p}) = \ln\left(\varepsilon_{0} \times \exp\left(\left(\frac{\rho}{N}\right)^{\beta}\right)\right)$$

$$\ln(\varepsilon_{p}) = \ln(\varepsilon_{0}) + \ln\left(\exp\left(\left(\frac{\rho}{N}\right)^{\beta}\right)\right)$$

$$\ln(\varepsilon_{p}) = \ln(\varepsilon_{0}) + \left(\frac{\rho}{N}\right)^{\beta}$$

$$\left(\frac{\rho}{N}\right)^{\beta} = \ln(\varepsilon_{p}) - \ln(\varepsilon_{0}) = \ln\left(\frac{\varepsilon_{p}}{\varepsilon_{0}}\right)$$

$$\frac{\rho}{N} = \left(\ln\left(\frac{\varepsilon_{p}}{\varepsilon_{0}}\right)\right)^{\frac{1}{\beta}}$$

$$N = \frac{\rho}{\left(\ln\left(\frac{\varepsilon_{p}}{\varepsilon_{0}}\right)\right)^{\frac{1}{\beta}}}$$

Physical meaning of the parameters:

$$\varepsilon_p = \varepsilon_0 \exp\left(-\left(\frac{\rho}{N}\right)^{\beta}\right)$$

where

 ε_p = Axial permanent strain

N = Number of loading cycle

 ε_0 , ρ , β = Material parameters that are different for each samples

 ρ and β = Parameters influencing the shape of the curve

TC-710-4-4-8

APPENDIX B **MATERIAL MODEL PARAMETERS**

Tseng and Lytton (1989) **B.1**

B.1.1 **Boral Warrians Quarry Base Material**

Table B 1: Boral Warrians (N₀ = 0 cycles)

Material	DDa	DOSa	MCa	ε ₀ (%)	ρ	β	Mean residual	Stdev residual	R ²
Warrians 98% Stad.	2.336	53	4.8	17.37 ± 2.8	1.16E+03 ± 5.3E+02	3.44 ± 0.38	0.185	0.117	0.998
	2.338	56	5.1	17.31 ± 3.3	1.49E+03 ± 6.9E+02	3.84 ± 0.45	0.176	0.135	0.997
	2.345	58	5.2	25.22 ± 3.3	1.10E+03 ± 4.4E+02	3.10 ± 0.26	0.145	0.119	0.999
Warrians 100% Std.	2.384	62	5.1	14.42 ± 1.9	1.64E+03 ± 4.9E+02	4.06 ± 0.32	0.089	0.075	0.998
	2.388	65	5.3	20.68 ± 2.4	1.50E+03 ± 5.7E+02	2.89 ± 0.22	0.101	0.094	0.999
	2.377	69	5.8	27.58 ± 3.1	9.80E+02 ± 3.2E+02	3.13 ± 0.20	0.110	0.102	0.999
Warrians 102% Std.	2.439	63	4.6	9.28 ± 3.6	1.57E+03 ± 1.7E+03	3.42 ± 0.83	0.175	0.144	0.988
	2.436	70	5.1	19.24 ± 2.3	1.69E+03 ± 4.9E+02	3.84 ± 0.28	0.111	0.084	0.999
	2.436	75	5.5	28.49 ± 3.8	9.74E+02 ± 2.8E+02	4.18 ± 0.31	0.158	0.115	0.999
Warrians 104% Std.	2.491	86	5.5	16.31 ± 2.2	1.69E+03 ± 5.4E+02	3.83 ± 0.30	0.099	0.082	0.999
	2.492	89	5.7	21.63 ± 1.4	1.59E+03 ± 2.7E+02	3.61 ± 0.15	0.064	0.062	1.000
	2.489	94	6.1	31.34 ± 1.8	1.33E+03 ± 1.9E+02	3.52 ± 0.11	0.058	0.054	1.000
Warrians 98% Mod.	2.372	59	5	18.86 ± 2.9	1.71E+03 ± 6.5E+02	3.68 ± 0.33	0.128	0.111	0.998
	2.376	63	5.3	22.35 ± 4.0	1.11E+03 ± 7.1E+02	2.71 ± 0.34	0.210	0.108	0.998
	2.365	72	6.2	49.98 ± 14.8	9.53E+02 ± 8.7E+02	2.57 ± 0.32	0.188	0.122	0.998
Warrians 100% Mod.	2.422	67	5.1	19.88 ± 1.6	1.42E+03 ± 3.2E+02	3.35 ± 0.17	0.063	0.085	1.000
	2.417	76	5.8	21.52 ± 1.8	1.43E+03 ± 3.7E+02	3.10 ± 0.17	0.080	0.081	1.000
	2.423	79	6	27.82 ± 1.8	1.25E+03 ± 2.5E+02	2.99 ± 0.12	0.072	0.050	1.000
Warrians 102% Mod.	2.470	74	5	17.85 ± 4.5	2.00E+03 ± 9.1E+02	4.83 ± 0.63	0.156	0.121	0.995
	2.465	80	5.5	20.61 ± 1.8	1.32E+03 ± 2.6E+02	4.17 ± 0.23	0.106	0.080	0.999
	2.469	84	5.7	27.10 ± 4.7	1.30E+03 ± 4.4E+02	4.63 ± 0.45	0.216	0.147	0.997

B.1.2 Karreman Quarry Base Material

Table B 2: Karreman material: Tseng and Lytton model parameters (No = 0 cycles)

Material	DDa	DOSa	MCa	ε ₀ (%)	ρ	β	Mean residual	Stdev residual	R ²
Karreman 98% Std.	2.165	65	5.9	22.69 ± 3.3	1.19E+05 ± 4.7E+04	0.35 ± 0.03	0.178	0.174	0.998
	2.169	59	5.3	36.76 ± 12.0	9.67E+04 ± 1.1E+05	0.24 ± 0.04	0.212	0.189	0.997
	2.164	56	5.1	53.24 ± 24.5	9.50E+04 ± 1.4E+05	0.24 ± 0.05	0.271	0.180	0.996
Karreman 100% Std.	2.208	55	4.5	16.50 ± 4.5	2.01E+05 ± 1.1E+05	0.46 ± 0.07	0.170	0.118	0.994
	2.212	60	4.8	20.80 ± 2.7	1.23E+05 ± 3.3E+04	0.46 ± 0.04	0.164	0.139	0.998
	2.210	66	5.3	30.11 ± 3.1	1.01E+05 ± 3.0E+04	0.30 ± 0.02	0.095	0.082	1.000
Karreman 102% Std.	2.258	53	3.8	9.67 ± 3.9	1.71E+05 ± 1.0E+05	0.59 ± 0.12	0.143	0.116	0.984
	2.251	62	4.5	20.17 ± 6.2	2.04E+05 ± 1.1E+05	0.49 ± 0.08	0.213	0.157	0.993
	2.258	65	4.6	43.23 ± 12.5	9.57E+04 ± 3.6E+04	0.61 ± 0.08	0.252	0.162	0.995
Karreman 104% Std.	2.297	60	3.8	5.06 ± 4.0	2.07E+05 ± 2.7E+05	0.52 ± 0.20	0.135	0.080	0.954
	2.296	66	4.2	12.88 ± 2.9	1.60E+05 ± 7.0E+04	0.48 ± 0.06	0.107	0.138	0.995
	2.302	69	4.3	5.94 ± 2.9	1.51E+05 ± 1.4E+05	0.48 ± 0.14	0.151	0.104	0.975
	2.296	76	5	30.91 ± 5.0	1.25E+05 ± 3.3E+04	0.54 ± 0.05	0.178	0.144	0.998
Karreman 98% Mod.	2.260	61	4.3	7.48 ± 3.5	1.63E+05 ± 1.5E+05	0.45 ± 0.12	0.171	0.118	0.979
	2.263	66	4.6	7.83 ± 4.2	1.53E+05 ± 2.4E+05	0.33 ± 0.11	0.220	0.140	0.980
	2.261	71	5	11.32 ± 6.7	1.95E+05 ± 2.4E+05	0.43 ± 0.14	0.276	0.187	0.972
	2.256	82	5.9	23.03 ± 3.0	1.22E+05 ± 4.1E+04	0.37 ± 0.03	0.183	0.128	0.998
Karreman 100% Mod.	2.306	61	3.8	3.86 ± 2.6	1.58E+05 ± 2.3E+05	0.43 ± 0.17	0.139	0.085	0.956
	2.314	68	4.1	1.49 ± 0.5	1.07E+05 ± 3.3E+05	0.11 ± 0.03	0.033	0.027	0.993
	2.306	81	5	10.41 ± 4.6	1.81E+05 ± 1.4E+05	0.50 ± 0.12	0.179	0.144	0.982
	2.309	90	5.5	30.21 ± 5.0	9.86E+04 ± 4.7E+04	0.31 ± 0.03	0.165	0.122	0.999
Karreman 102% Mod.	2.352	79	4.2	8.12 ± 3.5	1.62E+05 ± 1.5E+05	0.42 ± 0.11	0.167	0.130	0.983
	2.357	84	4.4	3.68 ± 2.2	1.22E+05 ± 2.2E+05	0.31 ± 0.13	0.128	0.079	0.976
	2.357	89	4.7	6.07 ± 2.2	1.39E+05 ± 1.3E+05	0.37 ± 0.09	0.127	0.088	0.988
	2.354	96	5.1	22.13 ± 5.6	2.06E+05 ± 8.7E+04	0.51 ± 0.06	0.165	0.154	0.995
	2.345	99	5.4	18.23 ± 2.3	1.14E+05 ± 3.8E+04	0.37 ± 0.03	0.148	0.111	0.998

APPENDIX C MODELLING THE EFFECT OF MOISTURE

The permanent deformation of granular materials and the effect of moisture content has been studied in the laboratory with the objective of providing mathematical models for the description of the impact of the moisture content on the performance of UGM.

Ba et al. (2015) undertook an extensive study to adjust the Tseng and Lytton material model for five different unbound granular materials. Experiments were undertaken at different moisture contents, and the sensitivity of the parameters to the moisture content was examined. A qualitative examination of the moisture content sensitivity, and its correlation with the Soil-water characteristic curve (SWCC), was performed.

The testing was performed at densities between 95%, and 98% of Modified MDD and moisture sensitivity was investigated at OMC and OMC \pm 2%. Moisture contents around OMC and above are, however, not very representative of the field conditions.

The moisture sensitivity on the permanent deformation reached after 100 00 cycles $\varepsilon_p(N=10^5)$ is shown in Figure C 1. Ba et al. fitted an exponential relationship for the effect of gravimetric moisture content. The exponential form selected has the following mathematical relationship (Equation 16):

$$\varepsilon_p^{\text{(N = 100 000 cycles)}} = a_0 \times \exp(a_1 w)$$
 20

where

 $\varepsilon_p(N=10^5)$ = Axial permanent deformation reached after 100 000 cycles

w = Gravimetric moisture content (%)

Moisture content sensitivity parameters. a_0 is the value of the

 a_0 and a_1 = deformation after 100 000 cycles when the moisture content tends

toward 0. a_1 represent the moisture sensitivity

At the first cycle At 100,000 cycles At the first cycle At 100,000 cycles 0.004 0.012 Diack Basalt Bakel Black Quartzite (mm/mm) after 100,000 cycles (mm/mm) 0.0035 0.01 = 0.00046974 * e^(0.50049W) 0.00010987 $R^2 = 0.40385$ 100,000 cycles 0.003 0.008 0.0025 0.006 0.002 0.004 0.0015 0.002 8. q.f. 0.00071582 0.001 2 2 Water content, W (%) Water content, W (%) -At the first cycle - At 100,000 cycles At the first cycle
At 100,000 cycles after 100,000 cycles (mm/mm) Bandia Limestone Bargny Limeston 100,000 cycles (mm/mm) e^(1,0688W) **S**) 1.5894e-6 * e^(0.70752W) $R^2 = 0.94405$ $R^2 = 0.98053$ 0.006 2.2264e 6 * e^(0.68401W) 0.004 R2= 0.98342 after, 0.002 5.5 Water content, W (%) Water content, W (%)

Figure C 1: Effect of moisture content on the RLT permanent deformation reached after 100 000 cycles $(\sigma_c = 35 \text{ kPa and } \sigma_d = 103 \text{ kPa})$

Source (Ba, Tinjum & Fall 2015).

Page 49 TC-710-4-4-8